VĚDECKÉ SPISY VYSOKÉHO UČENÍ TECHNICKÉHO V BRNĚ

Edice Habilitační a inaugurační spisy, sv. 738
ISSN 1213-418X

Alexandr Knápek

ADVANCED METHODS AND MATERIALS FOR RESEARCH AND DEVELOPMENT OF FIELD EMISSION EMITTERS

BRNO UNIVERSITY OF TECHNOLOGY
FACULTY OF ELECTRICAL ENGINEERING AND COMMUNICATION
DEPARTMENT OF PHYSICS

Ing. Alexandr Knápek, Ph.D.

ADVANCED METHODS AND MATERIALS FOR RESEARCH AND DEVELOPMENT OF FIELD EMISSION EMITTERS

POKROČILÉ METODY A MATERIÁLY PRO VÝVOJ A VÝZKUM AUTOEMISNÍCH KATOD

HABILITATION THESIS SUMMARY

VYSOKÉ UČENÍ TECHNICKÉ V BRNĚ
NAKLADATELSTVÍ VUTIUM

BRNO 2022

KEYWORDS
field emission of electrons, field emission emitters, polymer graphite, noise spectroscopy, orthodoxy testing

KLÍČOVÁ SLOVA
vlastní emise elektronů, autoemisní zdroje elektronů, polymerní grafit, šumová spektroskopie, ortodoxní testování

LOCATION OF THE THESIS
Department of Science and International Relations,
Faculty of Electrical Engineering and Communication,
Technická 3058/10, 616 00 Brno

ISBN 978-80-214-6101-7
ISSN 1213-418X

CONTENTS

CURRICULUM VITAE

Ing. Alexandr KNÁPEK, PhD. was born on 12th Dec. 1983 in Brno (Czechoslovakia). Alexandr Knápek is a graduate of the bachelor's degree program in "*Teleinformatics*" and master's degree in "*Telecommunication and Information Technology*" at the *Faculty of Electrical Engineering and Communication* (FEEC). In September 2008, he started to study the PhD program entitled "*Physical Electronics and Nanotechnology*" at the *Department of Physics* of the FEEC. He defended his PhD thesis in April 2013. The topic of his PhD. dissertation was related to the improvement of classical field-emission cathodes which were coated with a new type of dielectric thin layer, working as a quantum barrier and thus improving the electron emission from the surface. Dr. Knápek currently continues and extends existing research on cold field-emission electron sources and cold field-emission structures at the *Institute of Scientific Instruments* (ISI) of the *Czech Academy of Sciences* (CAS). In parallel, he continues his professional collaboration with the *Dept. of Physics* of the FEEC, where he has published a number of impacted publications till now.

The author's teaching activities at the BUT include teaching of *Physics 1*, *Physics 2* and *Physics Seminary* courses. Outside of the BUT, the applicant lectured as a guest-professor at the East Bavarian Technical University (OTH), where in the winter semester 2020/21 he lectured the *Advanced Optoelectronics* along with a course on *Vacuum Systems Technology*, and an intensive inter-semestral course on *Fundamentals of Electron Beam Lithography*. At his home institute (ISI), the author has long been supervising bachelor and master theses for the faculties of FEEC and at the *Faculty of Mechanical Engineering* (FME). Since 2016, the author is also a long-time member of the state-examination committee at the *Dept. of Microelectronics* of FEEC and is an external master's thesis supervisor to *Mu'tah University* in Al-Karak, Jordan, which is a partner university to which ISI connected by a contract.

Hence, during the last 5 years, Dr. Knápek has supervised 4 bachelors, 3 master and one PhD student at Dept. of Physics of FEEC and actively collaborating on publishing common impacted papers. As for the papers, Dr. Knápek has authored or co-authored 70 publications and has an H-index of 6 (excluding self-citations) according to the WoS/Scopus.

During his career he has worked on several international and national projects. He currently works on the four-year TAČR Trend project in collaboration with *NenoVision company*, with the *Faculty of Mechanical Engineering* and the *Institute of Physics of Materials*. The title of the project is "*Development of in-situ techniques for the characterization of materials and nanostructures*". It should be also mentioned that Dr. Knápek has more than a decade of experience in electron field-emission microscopy, and the related field of field-emission cathode preparation and characterization methodologies. In addition, author is also involved in surface diagnostics and microscopy and electron lithography.

INTRODUCTION

Field emission, also called as *Cold Field Emission* is a discharge of electrons to escape through a surface of a given material subjected to a strong electric field. The material surface acts here as a *barrier* to electron passage. In the mathematical form, the Field electron emission (FEE) process was introduced for the first time by R. H. Fowler and L. W. Nordheim, when they supposed that the nature of FEE is a *deep quantum tunneling* process from an exact triangular potential energy barrier. These assumptions were later modified by Nordheim who considered the existence of the image potential energy for the electrons, which changed the shape of the potential barrier yielding approximately triangular potential energy barrier, often called the *Schottky-Nordheim barrier* [1],[2]. This effect is utilized in the field-emission electron microscope (FEM), which in some instances achieves resolution of atomic dimensions [3].

Research on the phenomenon of field electron emission and especially the implementation of this phenomenon in the subject of field emission sources of free electrons from solids to vacuum is an *interdisciplinary problem* that can be addressed at many levels. The methods presented in this thesis map the results of my work in the field of cold field emission and can be broadly divided into *production methods* and *characterization methods*. The first group of the methods deals with laboratory preparation of the field emission structures using classical approach which is based on electrochemical formation of a sharp tip from a metal wire. The first group of methods mentioned also includes an up-to-date approach which incorporates a combination of state-of-the-art *lithography techniques* and modern *nanotechnologies* to fabricate nanotube-based emitter embedded in a gated structure. Special attention is paid to seek out for a new cathode material, which can be used to advantage in both approaches. I was particularly interested in modern *nanomaterials* and *nanocomposites*; specifically, I focused on tungsten oxide-based nanowires and polymer graphite.

The second group of methods is based on *in-situ testing* and *characterization*. The *in-situ* condition is a fundamental requirement, because in common daily practice it is not possible to remove the emitter out of the vacuum chambre. For these reasons, the methods presented in this thesis concentrate on measurement of current-voltage analysis which provide the required information about cathode function. Both methods therefore work with magnitude of *recorded total emission current* collected by faraday cage or by coated scintillator, relative to the extraction and/or acceleration voltage. The first analytical method is based on the application of *noise spectroscopy*, where the noise and fluctuations of the total emission current are monitored. The second of the analytical methods is based on the evaluation of the slope of the recalculated current-voltage characteristics, such as the *Fowler-Nordheim* plot, *Milikan-Lauritsen* plot or the *Murphy-Good* plot.

The two groups of methods presented form the necessary basis for the experimental development and characterization of cold emission emitters. The methods provide advanced solutions and implement latest technologies in areas where standard solutions do not exist or are very complicated. The methods thus contribute to the search for an ultimate electron source with high beam current density, high electron beam brightness and narrow energy bandwidth.

1. ADVANCED METHODS OF PRODUCTION OF COLD FIELD EMITTERS

To create a cathode or structure with the desired field emission parameters, it is first necessary to select a suitable cathode material. The criteria necessary to ensure its functionality are high melting point, low work function, high mechanical strength, and low chemical affinity.

Currently, a single-crystalline tungsten remains the widely used cathode material precisely because it meets all these criteria except for work function [1],[4]. The average work function of tungsten (4.5 eV) is slightly higher than that of other transition metals that generally appear to be suitable as well. Work function of a metal, which is the primary parameter affecting the ability of the electron to tunnel from the surface to the vacuum, can be affected by coating it with a thin layer, that is usually oxide-based or dielectric-based [A1]. Secondly, it is necessary to ensure a suitable shape of the cathode itself, and to ensure a suitable arrangement of the cathode relative to the extraction electrode or directly relative to the anode [3],[5],[8]. The shape of the cathode tip is related to the electric field distribution on the cathode surface, where a sufficient current gradient needs to be obtained [6].

1.1 REPRODUCIBLE ELECTROCHEMICAL TIP FORMATION METHOD

The most widely used method of forming an extra sharp tip is based on anodic dissolution [A1], [6], [7]. Although the anodic dissolution is an elementary chemical concept, the method of preparing the sharp tip is rather more complicated and there is no standardized, generally available instrumentation for which this theory can be fine-tuned. The situation is even more complicated when polycrystalline wire is used instead of single-crystalline wire, which is a highly desirable material for research development and laboratory work, due to lower price of the material [A1], [6]. For this purpose, a computer-driven tip etching method has been proposed to achieve mainly the good repeatability and to keep the ease of use [A2]. The programmable etching set-up described in [A2] is illustrated in Figure 1.1, the Electrical schematic of the etching set-up is illustrated in the same paper [A2].

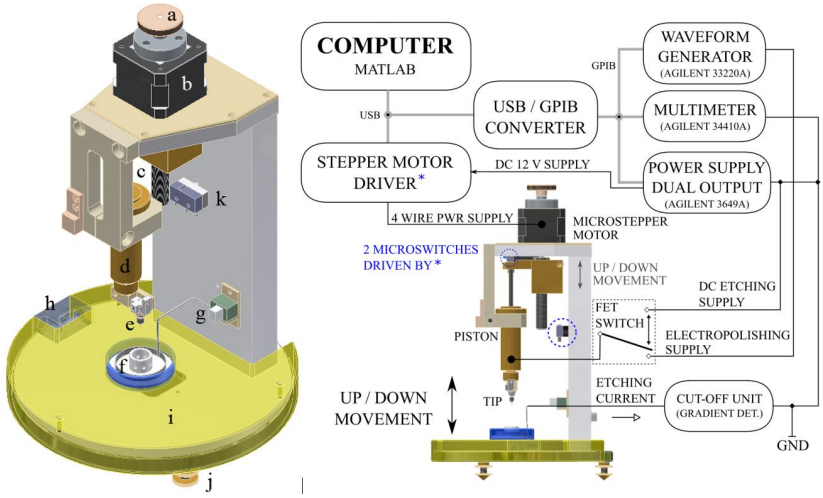

Figure 1.1 A model of the mechanical holder driven by a precise micro-stepper motor [A2].

The implemented etching method is based on a principle of anodic dissolution of a metal electrode (wire) in liquid electrolyte with voltage applied. The newly invented block illustrated in Figure 1.1, the so-called gradient detector is of highest importance.

Its purpose is to instantly disconnect the etching current and thus prevent the tip blunting that may appear. As shown in Figure 1.2 which describes the control algorithm of the production method, the cut-off algorithm is implemented at the end of the two-step method based on the calculation of the second differentiation in real-time.

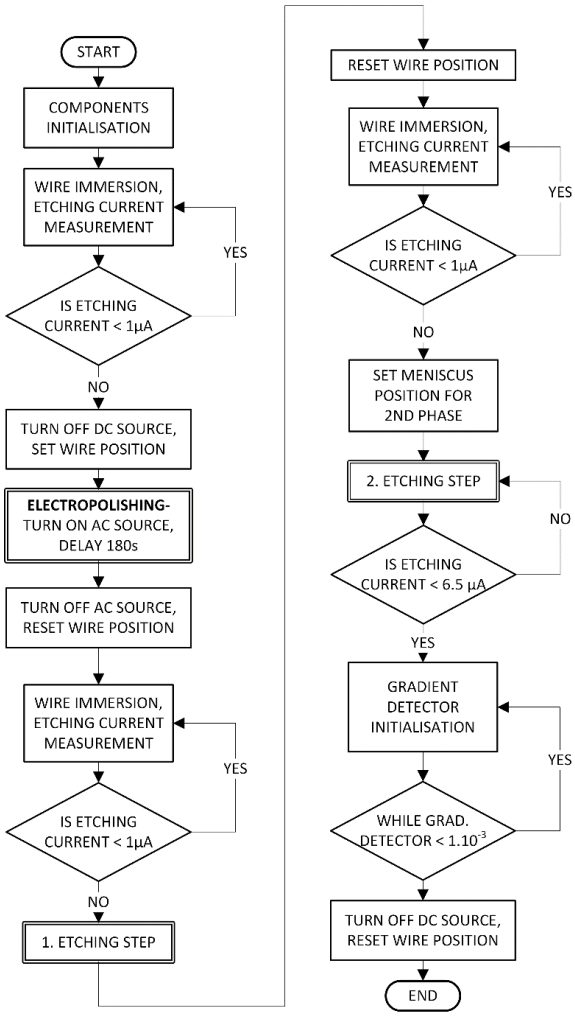

Figure 1.2 A flowchart representing the control software [A2].

For a polycrystalline tip illustrated in [A2], the tip reproducibility is rather high, which is illustrated by relatively low variance of the taper angle that is equal to 0.05 for our testing set of 100 tips. For single crystalline tips, due to homogenous etching rate caused by uniform crystalline orientation, the variance of the taper angle is even lower allowing to achieve an almost 100% reproducible tip. The previously mentioned utility model [A13] protects the technical solution developed to implement this methodology.

1.2 FABRICATION AND EVALUATION METHOD FOR A GATE STRUCTURE BASED ON E-BEAM LITHOGRAPHY

The designed system is based on a triode configuration incorporating an extractor enabling the field strength on the tip to be easily changed as illustrated in Figure 1.3. Such arrangement provides significant versatility as it can can be used with a different kind of nanotubes or nanowires implanted to work as the cathode.

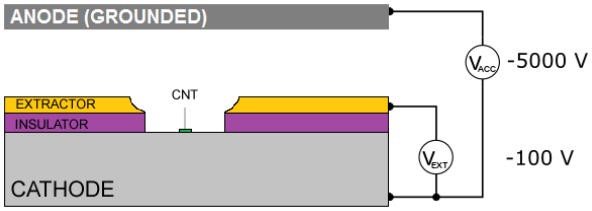

Figure 1.3 Fabricated gate structure including an example of wiring [A3].

As a feature of this structure, the extraction voltage can be adjusted within a range from zero to approx. 1 kV. When used for a CNT cathode, the radius of the cathode is influenced mainly by the size of the catalytic iron particle from which it grows. The described gate structure is prepared using electron beam lithography and reactive ion-etching that are suitable for this task [A3],[10],[11]. The preparation method consists of the following fifteen technological steps as it is illustrated in Figure 1.4.

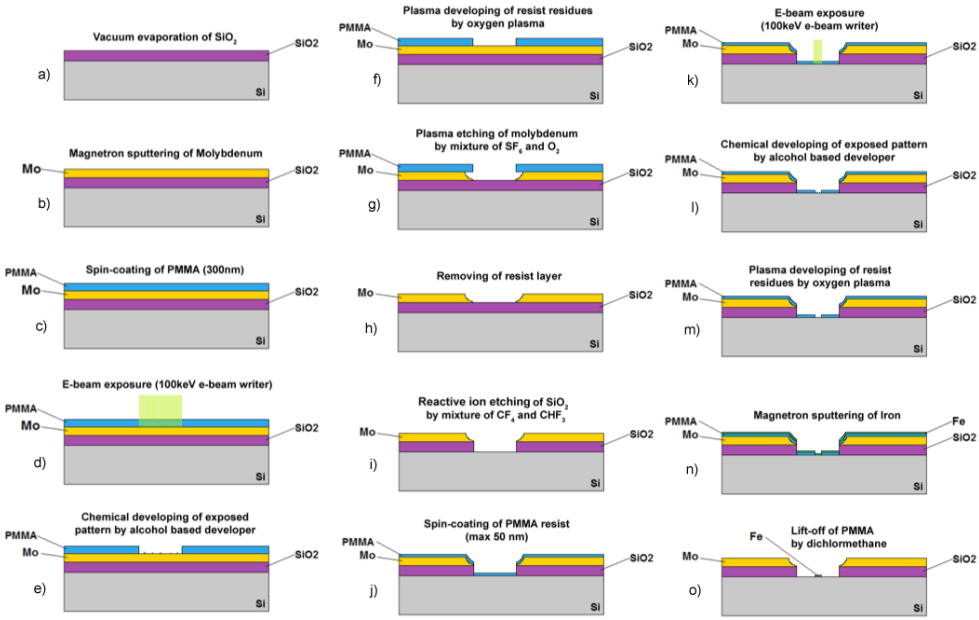

Figure 1.4 Fabrication technology of the gate structure: the fifteen basic steps (a-o) [A3].

The usual lithography steps are performed to prepare the layer of catalytic iron particles: Spin-coating of PMMA resist, E-beam exposure of the pattern and its chemical developing by an alcohol-based developer, followed by plasma developing of resist residues using oxygen plasma. A thin layer of catalytic particles is sputtered after the residues are developed, followed by the lift-off of the PMMA and the PECVD process used for CNT growth.

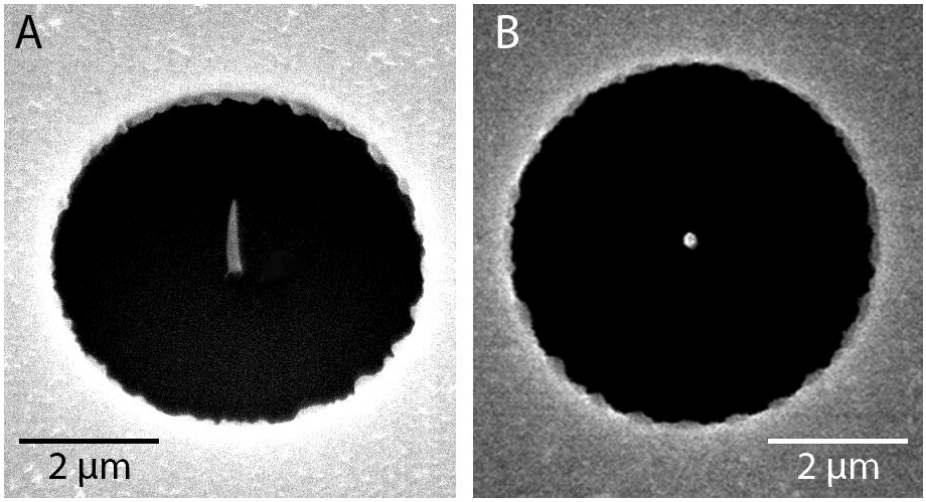

Figure 1.5 SEM image obtained by magnifying the structure 10,000x illustrating the side view of the Pt nanorod embedded gate structure (A) and the top view (B) [A4].

The above located Figure 1.5 illustrates a model structure with an aperture size of 5 µm which is fitted with a platinum nanorod fabricated using electron beam assisted deposition [A4],[14]. The imaging was performed using a scanning electron microscopy branded JEOL JSM-7001F.

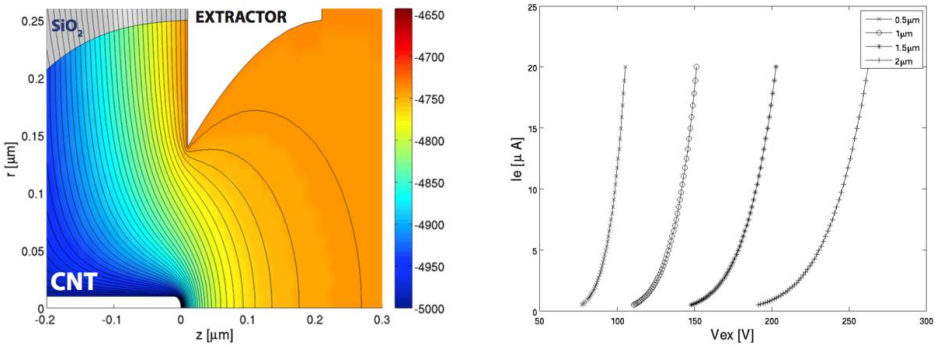

Figure 1.6 Potential in the vicinity of the cathode (left) for a system with a bore diameter of 250 µm computed as a function of the extraction voltage for several bore diameters (right) [A3].

The CNT sources work at room temperature and a high field, so the emission is well described by the thermal-field emission model [13] which is a generalization of the standard cold field emission model.

The electrostatic field in the system was computed using the first order finite element method (FEM). We used a triangular mesh which is sufficiently dense in the vicinity of the CNT with a tip diameter of 20 nm, and which expands in other parts of the system. The field calculation took about five minutes with a mesh consisting of about a million triangular elements. The emission was studied for several extractor bore diameters within a range from 0.5 to 2 µm. The typical potential in the vicinity of the cathode is plotted in Figure 1.6 (left). The emission current can be computed as a function of the extraction voltage using a thermal field emission model; Figure 1.6 (right).

As the size of the CNT source is very small the energy distribution and brightness are strongly influenced by the stochastic Coulomb interactions (CI) in the beam. Their effect on the energy distribution was simulated using a Monte-Carlo simulation presented in [13] yielding the emission energy width of the beam (Figure 1.7, left) and the axial reduced brightness (Figure 1.7, right). The effect of the bore diameter in the extractor was analyzed using another MC simulation: (a) The initial conditions of emitted electrons were randomly generated to fulfill the theoretically computed current density j_{TF} and the energy distribution in the thermal field emission regime [A3]. (b) The electrons were traced through the system field including the effect of the stochastic CI.

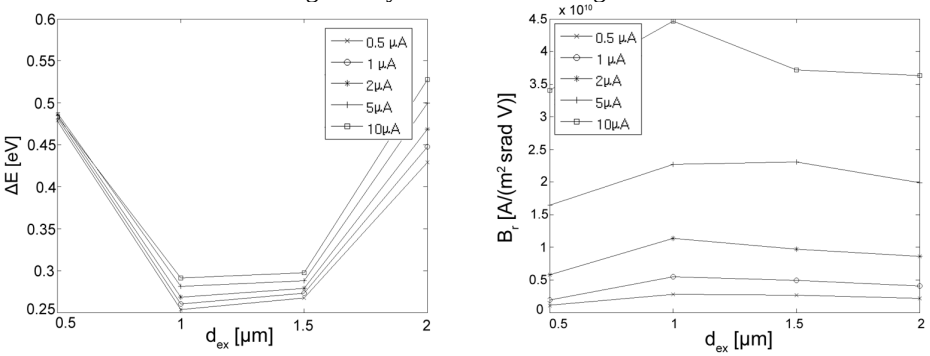

Figure 1.7 The emission energy width – FW50 (left) and the axial reduced brightness (right) with respect to the emission current for several bore radii [A3].

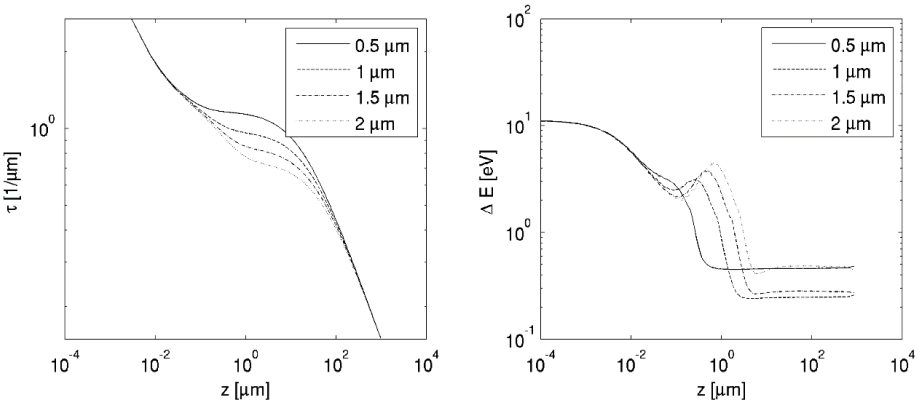

Figure 1.8 Linear electron density around the optical axis for several bore radii and the emission current 1 μA (left), energy width of the beam in planes perpendicular to the optical axis for several bore radii and emission current 1 μA (right) [A3].

The resulting energy width and the reduced brightness were computed from the beam properties in the anode plane. The effect of the stochastic CI is proportional to the electron density in the vicinity of the cathode which decreases with increasing bore diameter; Figure 1.8 (left). On the other hand, the equipotential lines are more curved with increasing bore radius which leads to higher energy width in each plane perpendicular to the axis; Figure 1.8 (right). In the region close to the extractor plane the particles that are further from the axis are accelerated by different potential differences than particles near the axis. This increases the effect of the stochastic CI. The results presented in Figure 1.7 show that the optimal value of the bore diameter is between 1 and 1.5 micrometers, where the maximal brightness and the minimal energy width were achieved for all emission currents.

2. NOVEL MATERIALS FOR COLD FIELD EMITTERS

2.1 COLD FIELD EMISSION FROM GRAPHITE SURFACE

In the paper [A5], we were the first to measure and describe the field emission behavior from the surface of exfoliated highly ordered pyrolytic graphite (HOPG) correlating it with the sample's topography that was obtained using SEM and AFM. A sample of single-crystalline HOPG of a ZYA grade, was used for the experiment. The upper layers of HOPG were mechanically exfoliated using 3M adhesive tape and cleaned using ion bombardment and heating prior to electron microscopy observation in the adjacent ultra-high vacuum (10^{-8} Pa) chamber [A5]. To remove any possible contaminants that may have stuck to the surface, the HOPG slab was annealed to 900 degrees Celsius for 20 minutes by means of electron bombardment heating. After the cleaning procedure, the sample was moved via a feedthrough to the ultra-high vacuum chamber equipped for scanning low energy electron microscopy (SLEEM) [15]. There, the sample was connected to a negative DC source providing the necessary extraction voltage. The emitted electrons were collected by a cerium-doped Yttrium Aluminum Garnet (YAG:Ce) scintillator, allowing to measure the emitted current. A schematic arrangement is illustrated in Figure 2.1 [A5].

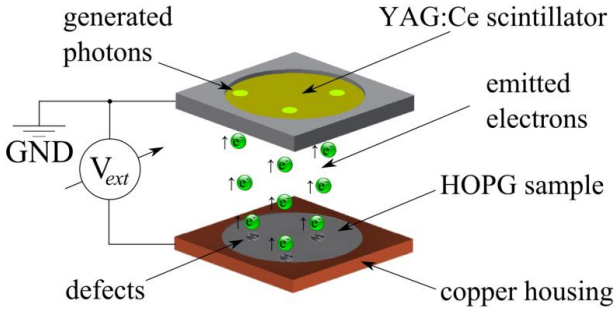

Figure 2.1 Experimental setup; the HOPG sample is connected to the negative dc source and the YAG scintillator is grounded, serving as an anode [A5].

The effect of field emission occurs only at disrupted surface, i.e., surface containing ripped and warped shreds of the uppermost layers of graphite. These deformations provide the necessary field gradients which are required for measuring tunneling current caused by field electron emission. Figure 2.2 (left) illustrates the I-V characteristics showing a nearly exponential increase of the current. Also, the Fowler-Nordheim plot (FN) Figure 2.2 (right) confirmed the presence of electron tunneling because of the nearly linear plot.

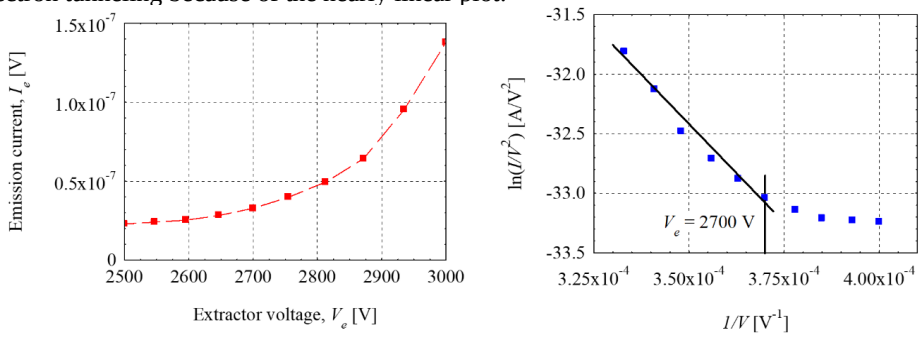

Figure 2.2 HOPG FE measurements: I-V characteristics of the emission current as a function of applied voltage (left); corresponding FN plot for the I-V characteristics (right) [A5].

As shown in Figure 2.2 (right) the non-linear behavior starts to appear at V_e = 2077 V suggesting the current contribution of larger defects, i.e., defects with lower field gradient. The nonlinearity of the plot can be explained by the presence of multiple microscopic electron sources. As each of them has a different geometry, the field gradient also differs, and with it the voltage necessary for the onset of field emission. This caused a gradual activation of individual sources making the I-V plot non-exponential [A5].

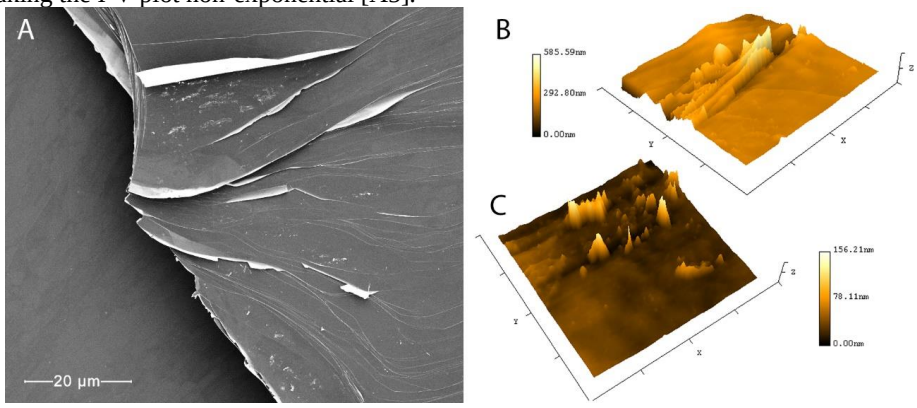

Figure 2.3 (A) SEM image of the HOPG surface. (B) AFM topography image of the HOPG surface showing the height of sample: a typical example of ridge-like morphological structures on the surface; (C) peak-like structures [A5].

The morphology of the shred was characterized by AFM and SEM. Typical shreds found on the sample surface are shown in Figure 2.3 (A) and (B). The SEM image shows an otherwise smooth HOPG surface with some partly exfoliated shreds. The shreds exhibit a layered structure with folds and corrugations. The results obtained in this paper became the basis for further experimental work on the polymer graphite described in Subsection 2.3.

2.2 COLD FIELD EMISSION FROM THE W_5O_{14} AND $W_{18}O_{49}$ NANOWIRES

Metal oxides have been often used to create so-called activation layer for a cold- or thermionic field emission cathode. For this reason, it makes good sense to try to create a nanotube (or generally a nanowire) from an oxide-based material and take advantage of its favorable material properties as they are introduced in the following paragraph.

In our paper [A6], we reported a comparative study of surface and field emission properties of W_5O_{14} and $W_{18}O_{49}$ nanowires (NWs) synthesized by a modified method using WO_3 and elemental tungsten as starting materials in the iodine transport method using nickel as a growth promotor. The method is in detail described here [22].

The crystalline structure of the NWs was examined by XRD at room temperature with D4 Endeavor diffractometer (Bruker AXS) using a quartz monochromatic Cu Kα1 radiation source (λ = 0.15 nm) and a Sol-X dispersive detector. Morphology, surface structure and work functions of W_5O_{14} and $W_{18}O_{49}$ NWs were measured by scanning electron microscope (SEM) Supra 36 V P, Carl Zeiss, scanning tunneling microscope (STM), atomic force microscope (AFM), and Kelvin probe operating in ultra-high vacuum (Omicron VT-AFM) [A6].

FE measurements in *microscopic regime* with both kinds of wires were carried out in the STM chamber at the same distance (approx. 2 μm) between a wire's apex and HOPG, which was used as an electron collector. The threshold voltages (onset voltages) for FE were determined from the minima of the corresponding Fowler–Nordheim (F–N) plots. After comparative testing, FE from a W_5O_{14} NW was studied also at distance of 4 and 5 μm [A6].

The comparative FE studies were performed on two wires with very different diameters in the same FE configuration. A W_5O_{14} NW, 14 μm long and 109 nm in diameter, was attached on a tungsten wire using FIB. The $W_{18}O_{49}$ wire, 247 μm in length and 4 μm in diameter, was attached on a Pt/Ir wire with silver epoxy paste. Then both tips were transferred into the UHV-STM chamber (7×10^{-10} mbar) and tested without any cleaning or annealing [A6].

Firstly, the so-called activation process was studied, in which the FE tips were cleaned of adsorbents and/or impurities. Figure 2.4 shows current-voltage (I–V) characteristics of the first (A) and the second (B) consecutive test and their corresponding F–N plots: a-b: W_5O_{14} NW, c-d: $W_{18}O_{49}$ wire. Firstly (A), the so-called activation process was studied, in which the FE tips were cleaned of adsorbents and/or impurities. Significant changes have been noticed in the onset voltages in two consecutive FE measurements, which dropped for both wires in the second test. A possible reason is the removal of adsorbates from the top end of the wires. Also, the knees in the F–N plots of the first tests can be explained with desorption of adsorbates under high electric fields [28].

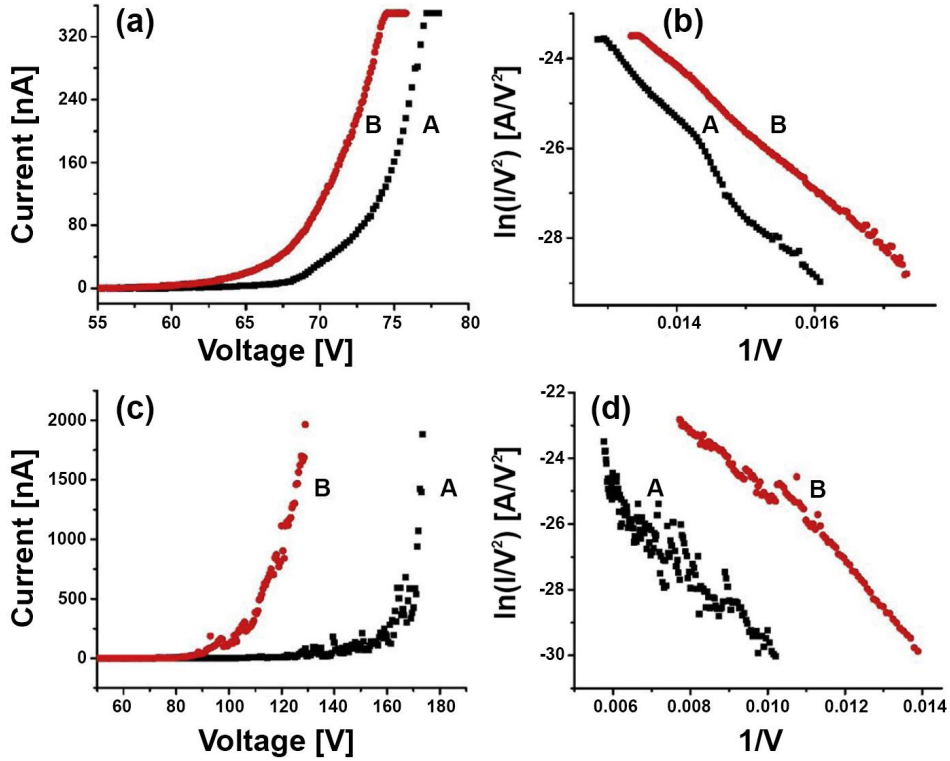

Figure 2.4 I–V curves and corresponding F–N plots: (a, b): W_5O_{14} NW; (c, d) $W_{18}O_{49}$ wire. The first tests are labelled with A, and the second with B. The measurements were performed at 2 μm [A6].

The FE experiments at macroscopic distances (≈ 1 mm) were performed in two configurations: the $W_{18}O_{49}$ NW in a negatively biased cathode and grounded anode configuration, and W_5O_{14} NW in a positively biased electron extractor configuration.

For the $W_{18}O_{49}$ NW, a 10 μm long and 180 nm in diameter, was attached on a tungsten electrochemically etched tip using FIB. The tip was annealed by the electron bombardment procedure for 15–20 min and flashed for 20 s. Thereafter, FE measurements of the $W_{18}O_{49}$ NW

were carried out at two distances: 600 μm and 800 μm from the Si wafer which served as a collection electrode.

Figure 2.5 shows the FE I–V characteristics for both distances and their corresponding F–N plots. At each position, FE experiments were performed three times to confirm repeatability. The FE currents were limited to 45 nA with the aim to prevent damage of the nanowire. The onset voltage of FE was 322 ± 1 V at 600 μm and 354 ± 1 V at 800 μm. The limit current was reached at 433 V and at 463 V, respectively (Figure 2.5.a). No significant differences were detected when the voltage was ramped up or down. In the F–N plots (Figure 2.5.b), the straight lines indicate the standard barrier-tunneling mechanism of the field electron emission. No degradation was observed. The field enhancement factors were determined using FN formalism incorporating the value of work function (i.e., 4.56 eV) experimentally obtained by KPFM. The field enhancement factors were 5050 ± 30 and 6450 ± 30 for 600 and 800 μm, respectively.

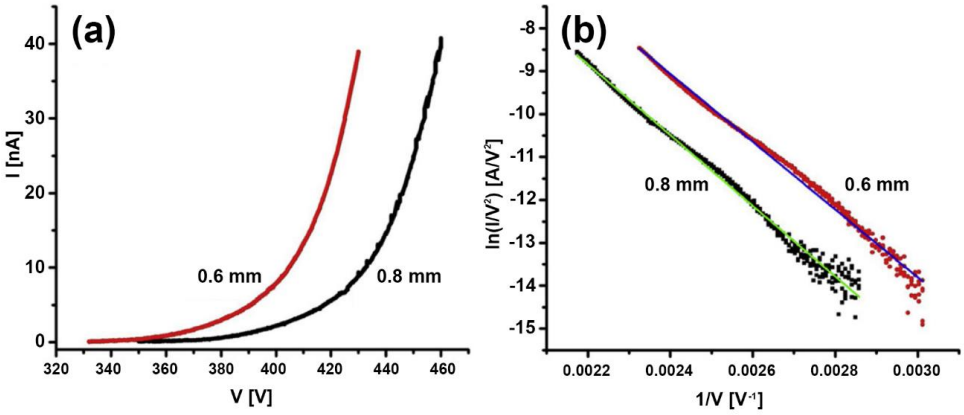

Figure 2.5 FE testing of a $W_{18}O_{49}$ NW at two distances (600 μm and 800 μm): a) I–V characteristics; b) The corresponding F–N plots with linear fits [A6].

The W_5O_{14} NW used in the macroscopic FE regime measurement was 5 μm long, 148 nm in diameter and mounted on an electrochemically etched tungsten wire by FIB. The experiment took place in an UHV chamber at 2×10^{-9} mbar with a separation of 1060 μm between the NW apex and the extractor plate. Three FE tests were performed. The voltage was manually increased step by step in 5 min intervals for the current to stabilize.

In the first test, the voltage was increased to 990 V and the corresponding FE current reached 183 nA. The I–V curve (Figure 2.6.a) is exponential and relatively smooth. The second test revealed the maximum FE current of 1.2 μA at 890 V, while at higher voltages the current started to decrease. The FE current (990 nA) at 990 V was more than 5 times larger (Figure 2.6.b) than in the first test. In the third test, the maximum current of 1.063 μA was obtained at a higher voltage as in the second test, i.e., at 1063 V, while at 990 V the current was 1008 nA, i.e., again larger than in both previous tests (Figure 2.6.c).

The explanation of the increase of FE current relate to the absence of cleaning of the emitters before FE testing. The subsequent tests gradually removed adsorbates from the NW, and the FE current consequently increased. Relatively high currents, which could cause diffusion of tungsten atoms and structural changes of the nanowire, could be the origin of degradation of the FE tip. Field enhancement factor from the F–N plot corresponding to the first test (Figure 2.6.d) was ≈ 17.000, while using the Eq. 3, it is 7 ± 0.5. The onset fields for three subsequent tests were 3.3 ± 0.3 V/μm, 3.4 ± 0.3 V/μ, and 3.5 ± 0.3 V/μm.

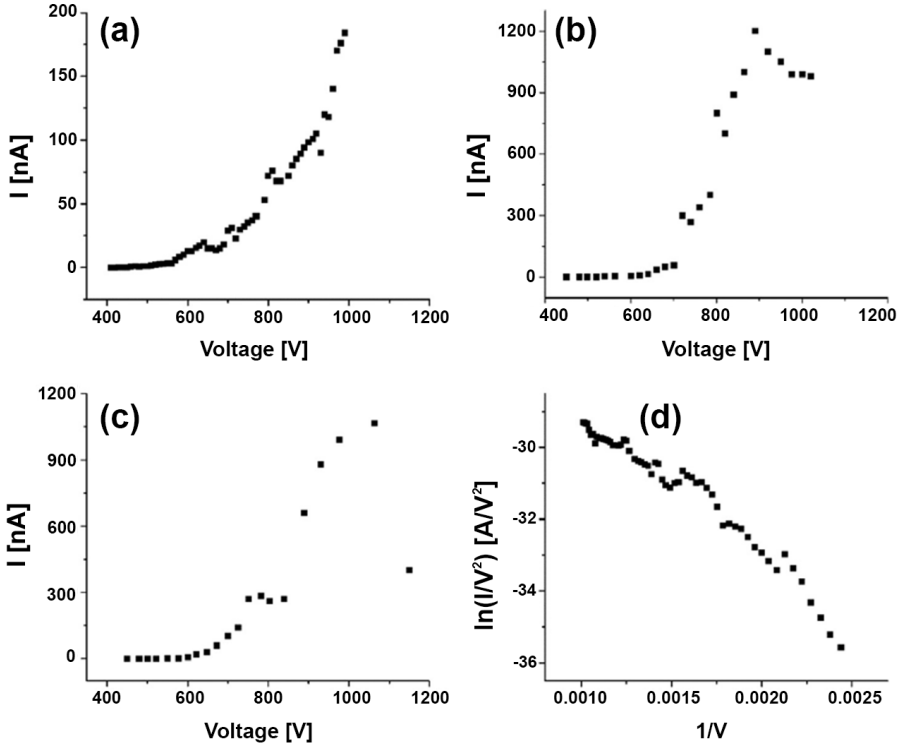

Figure 2.6 FE properties of a single W_5O_{14} NW in subsequent tests: a) the first test; b) the second test; c) the third test; d) F–N plot of the first test [A6].

In comparison to the $W_{18}O_{49}$ NW, the W_5O_{14} NW was found to be a more efficient field emitter because of its lower work function and lower onset voltage. The obtained results open several perspectives in utilization of tungsten oxide nanowires as a source of low-energy electrons in different devices. In particular, the W_5O_{14} NWs are promising with larger electric conductance and typically smaller diameter than $W_{18}O_{49}$ NWs, as well as due to relatively high field enhancement factors they can be activated at relatively low electric fields [A6].

2.3 COLD FIELD EMISSION FROM POLYMER GRAPHITE

Polymer graphite (PG) is a relatively young nanocomposite material that was invented mainly for micro-pencil refills containing a polymer-based binding agent and graphite flakes [A7],[A8],[A9]. Following the research on field emission from the HOPG surface presented in Chapter 2.1 and considering the favorable properties of graphite, it was logical to continue investigating this special composite form of Graphite, which pleasantly surprised us not only with its FE properties.

The PG has high conductivity and immunity against surface contamination, with a low price, which make it seem a highly suitable material for electrode manufacture in general [29],[30],[31]. Such pointed graphite rods may find various applications in analytical methods; for example, they can be used as a source of free electrons [A7],[A8] or they can operate with a tunneling current in Scanning Probe Microscopy (SPM) conductive modes [A9]. During our research, we described the material properties of polymer graphite from several manufacturers and presented 3 methods of tip formation, each of which is suitable for a different application.

The graphite pencil rods have generally two main constituents: graphite itself and various clay minerals or rocks, which are finely ground (small amounts of wax or polymers are also present to serve as a binder) [31]. In the paper, it was also reported that polymer graphite contains usually from 30% up to 80% of sp^3 hybridized carbon which may shift its properties more toward those of diamond-like carbon (DLC) structures. The macroscopic hardness of polymer graphite rod is determined by the graphite–clay ratio. An increase in the amount of clay will result in a harder rod that is therefore less smudgy when used on paper, whereas by reducing the amount of clay, a softer, more graphite-rich rod may be produced [A8]. The market of pencil leads consists of several popular brands of mechanical pencils (e.g., Pilot, Erich Krause, Proff, Parker, KOH-I-NOOR, Stabilo, Pentel, Staedtler, Faber-Castell, Rotring, Bic, Conte, Index, Lamy, Constructor, and many others). Each product is based on a special fabrication technology. For our experiments, we have used three different brands of polymer graphite rod, in particular: KOH-I-NOOR, Staedtler, and Pentel Hi-polymer E [A9].

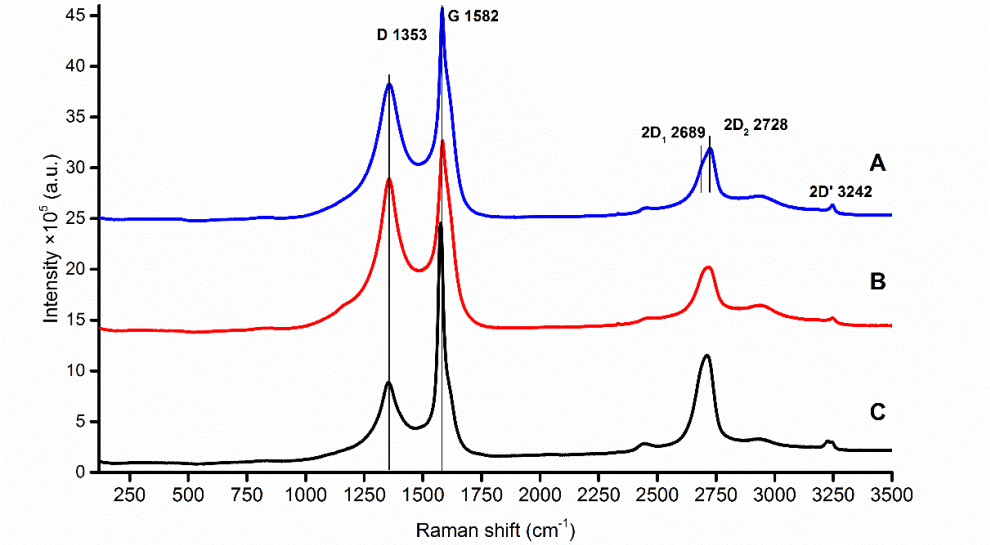

Figure 2.7 Stacked Raman spectra of each sample: Pentel Hi-Polymer E (blue), KOH-I-NOOR (red) and STAEDTLER (black) [A9].

The Raman spectra of pencil leads show peaks common in polycrystalline graphite, the G peak observed at 1580 cm^{-1}, which arises from the bond stretching of all pairs of sp^2 hybridized atoms, the D peak at around 1360 cm^{-1}, which becomes visible in relation with the defects in sp^2 graphite sheets, in polycrystalline graphite and graphite like materials with crystalline defects, D peak overtone called 2D peak is observed at around 2690 cm^{-1} and on polycrystalline graphite samples splits into two components $2D_1$ and $2D_2$ [33]. The above-mentioned measurements are illustrated in Figure 2.7 [A9].

D/G and $2D_1/2D_2$ intensity ratios [33] gives information about the estimated size and turbostraticity of layers of polycrystalline graphite flakes, which may play a significant role in the fabrication of sharp STM tip. The pencil leads were also thoroughly investigated using EDX and XPS with the aim to obtain complex information about both the surface and the bulk properties. Compositional analysis of different carbon leads was presented originally by Navratil et al. in [31] and Kariuki in [34].

Table 2.1 Properties of analyzed pencil leads, Raman I_D/I_G intensity ratio, calculated crystallite size, relative atomic concentration derived from XPS measurements [A9].

	Raman		EDX Contaminants		XPS [atomic %]				
Sample	**I_D/I_G**	**Crystallite Size [nm]**	**Side surface**	**Spot at the rod axis**	**C**	**O**	**Si**	**Fe**	**F**
Pentel	0.60	63	O, Na, Si, P, Fe	O, Na, Si, P, Zn	65.3	23.4	8.8	0.6	1.3
KOH-I-NOOR	0.36	101	O, Na, Mg, Al, Si, P, S, Cl, K, Ca, Fe	O, Na, Mg, Al, Si, P, S, Cl, K, Ca, Fe	67.2	23.9	8.0	0.7	-
Staedtler	0.35	102	O, Na, Mg, Al, Si, S, Cl, Ca	O, Na, Si, S, Cl, Ca	48.2	24.1	15.6	0.8	1.3

Properties of analyzed pencil leads incl. Raman ID/IG intensity ratio, calculated crystallite size and relative atomic concentration (derived from XPS measurements) are illustrated in Table 2.1.

Firstly, the tips were prepared by the means of focused ion beam (FIB). The FIB used was equipped to a commercially available SEM branded Helios of the former FEI company (now Thermofisher Scientific). We used preliminarily mechanically sharped probes to decrease the time of ion milling [A9]. Figure 2.8 shows that the tip apex diameter can go down to tens of nanometers, which is usually smaller than the size of a graphite flake. This is the uniqueness of this method, as it produces a compact tip whose FE parameters are practically identical to those of the metal. These findings are described in [A7]. Another disadvantage of a tip made in this way, and the main difference from the conductive behavior of metals, is the presence of impurities in the volume. Based on noise spectroscopy presented in [A7], it was found that the presence of these impurities causes quasiperiodic trapping and releasing of conduction electrons. Thus, the impurities behave as electron traps and contribute to the current fluctuations [A7].

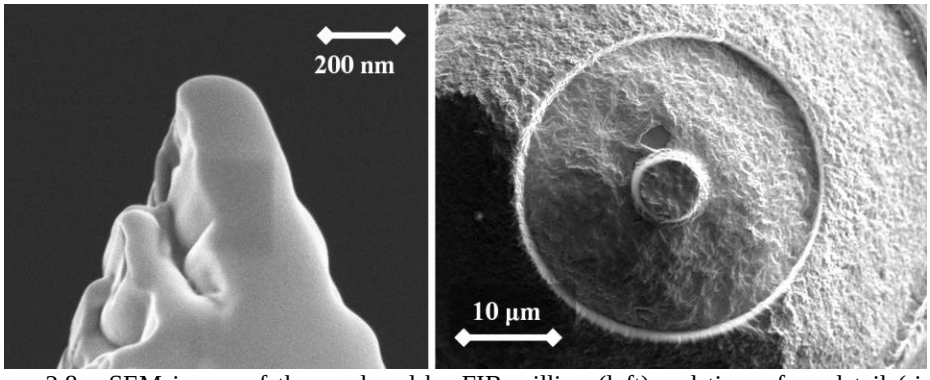

Figure 2.8 SEM image of the produced by FIB milling (left) and tip surface detail (right) showing graphite flakes from top before milling. Material used for this tip is STAEDTLER 0.3 HB [A9].

Another method of preparation that has been proved useful is based on mechanical grinding that has been achieved by a sanding as illustrated in Figure 2.9. That is the simplest method how to form a sharp tip on a PG rod. The only disadvantage is the low reproducibility of the probe's shape and absence of a sharping control-mechanism of the tip. The sharping could be carried out by grinding, for example, on a sandpaper or by forming with a sharpener [A9].

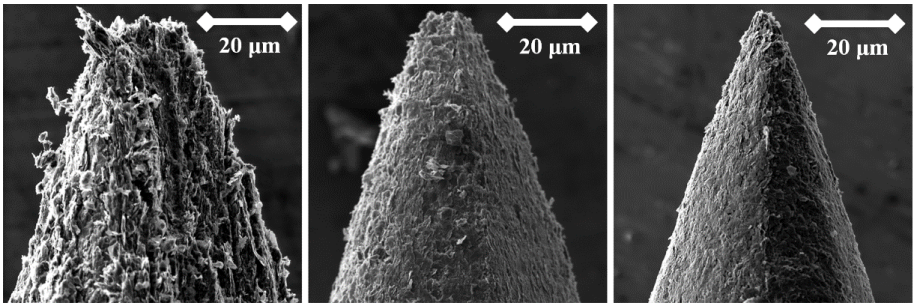

Figure 2.9 SEM image of the tip produced by mechanical sharping from the Hi-Polymer rod (left); by the mechanical sharping from KOH-I-NOOR rod (middle) and the mechanical sharping from Staedtler rod (right) [A9].

Apparently, the diameter of the tip prepared in this way is many times larger than conventional tips that are suitable for field emission of electrons; however, the presence of perpendicularly oriented flakes (with respect to the surface) allows this tip to be used as a large area field emitter (LAFE), with individual flakes serving as partial electron sources. Emitters based on mechanically ground tips are still under investigation.

The third method that has been tested for preparation of the graphite sharp tip is based on an electrochemical etching, as it was published earlier. Electrochemical method of tip preparation and sharpening provides good reproducibility of the tip shape and sharpness [A2]. Type and concentration of hydroxide (NaOH, KOH) along with the kind and voltage of an etching current allows controlling of tip etching rate and thus about the tip quality. The bulk of the graphite is most likely remained unreacted and precipitates on the metal ring in the form of flakes. The gas generation is illustrated in Figure 2.10 by etching current waveforms. There are two different waveforms for two different solutions etched by the same etching voltage (5V) showing quasiperiodic occurrence of peaks that are connected to the generation of bubbles. When a bubble is generated near the etched tip, the surface that is in connection with the etchant starts to be reduced and hence, the etching current starts decreasing.

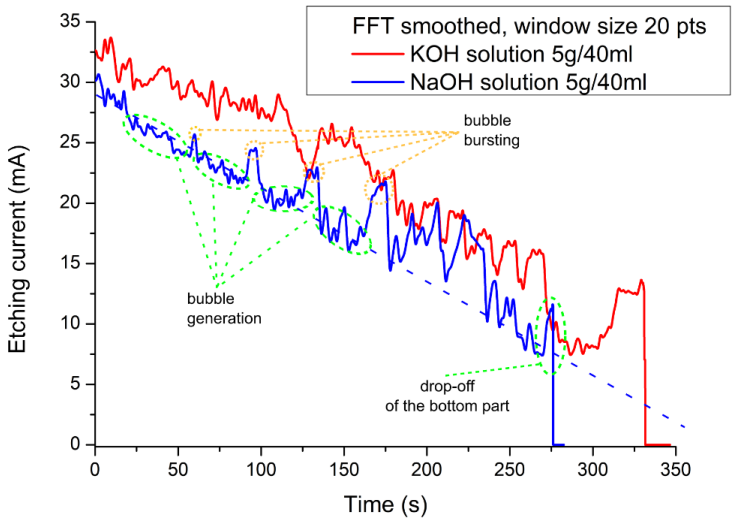

Figure 2.10 Etching current of a polymer graphite rod using two various etchants [A8].

The initial material-analysis of the polymer graphite tip, providing basic tip geometry and structure, was obtained by classical SEM. Those observations showed that the surface of electrochemically etched tip looks similar like the mechanically grinded tip and that also here, there are multiple graphite flakes oriented in various directions towards to the surface. Some of the flakes may have sufficient field gradient when connected to the negative power supply in the vacuum chamber of the FEM and act as a partial electron source. For these reasons, also this kind of tip is considered more like a field emission array of non-homogeneously distributed tips of different sharpness and hence different field enhancement.

As it will be discussed in more detail in section 3.3, to do the complete analysis of the surface of the a Large Area Field Emitter (LAFE) we need to extract two important characterization parameters which are the Macroscopic Field Enhancement Factor M – FEF (γ_M) and the Formal Area Efficiency (α_f^{SN}) for Schottky – Nordheim (SN) like potential barrier. To do these analyses the Murphy – Good plots were used to analyze the obtained data and to extract the characterization parameters for the emitter.

Figure 2.11 (left) presents the I-V characteristics of polymer graphite electron emitter in diode configuration that was measured in the field electron microscope and Figure 2.11 (right) presents the analysis plots for the 5 periods for the tested tip [A8]. Based on the result, this analysis also implied existence if multiple sources (sharp tips) that are sufficiently sharp to achieve field gradient strong enough to provide field emission current. This is in perfect agreement with the topographical analysis provided by the SEM showing multiple flakes oriented perpendicularly towards to the tip surface. Latter arrangement behaves similarly like general LAFE providing extended tunneling capabilities even for a tip of a relatively blunt diameter [A8]. More detailed explanation of the MG formalism will be given in the chapter 3.3.

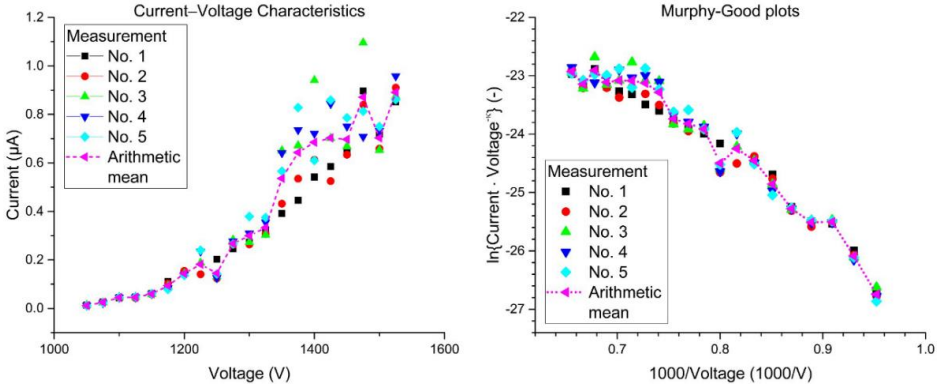

Figure 2.11 FE analysis of the electrochemically etched tip: the I–V Characteristics for the 5 measurement cycles (let) and the corresponding MG plots (right) [A8].

Another very interesting use of the polymer-graphite tip that has been found during the pursuit of the research is to use the polymer graphite a material to fabricate low-cost probes for SPM. The idea behind this is related to the replacement of PtIr alloy and tungsten, which are most used to produce SPM probes. Main characteristics of polymer graphite which could be found to be one of the most convenient for usage in scanning probe microscopy (SPM) are heat resistance, considerable durability, resistance to mechanical and hydraulic stress, and finally, the corrosion resistance [A9]. To test the functionality, three types of probes for SPM measurements were used: the tips prepared by electrochemical etching, by mechanical grinding and the tips prepared by FIB milling as described in previous paragraphs.

Each of the tip was successfully used for SPM images acquisition. The sharpness of all our tips proved to be sufficient; however, the sharpness depended strongly on the mark of the chosen pencil lead. The lowest sharpness was obtained by Pentel HiPolymer rod. KOH-I-NOOR and Stadler allows preparation of tip with small cultivate radius. FIB processing and chemical etching of the tips ensure reliable obtaining of the tips with demanded geometry. Nevertheless, even the mechanical sharping proved to sufficient during STM in air when sub-nanometer resolution is not demanded. The probes are also stable against oxidation and can be repeatedly sharped for continuous measurement by simple sharping procedure. The shape of the tip apex is usually created by a single flake of a graphite and determines the output quality of SPM while the precise shape of the tip does not play a significant role [A9].

To demonstrate the simplicity of working with PG probes, all the results presented were made by mechanically sharped tips that can be prepared almost effortlessly just by sharpening a PG rod by a sandpaper of high granularity (> 1600 grains/cm^2). The probes were tested within SPM NT-MDT Nanoeducator II. As a reference sample for estimation of our probes, a surface of a compact disc and highly oriented pyrolytic graphite (HOPG) were chosen (Figure 2.12, left). The HOPG surface (Figure 2.12, right) was used as reference sample for different types of electrical characterization in probe microscopy.

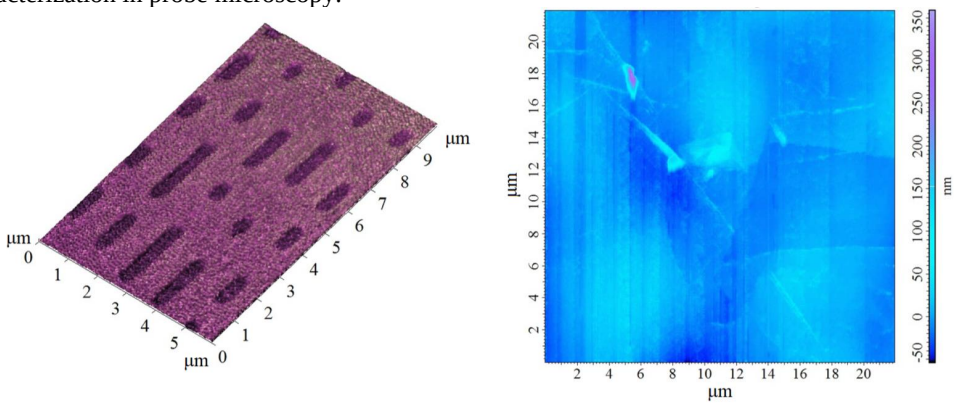

Figure 2.12 SPM image of the reference sample obtained by PG tip: (left) the surface of a compact disc and (right), the surface of a HOPG [A9].

Tip's performance was demonstrated on a SEM calibration standard. The standard contains grids of various sizes. For our measurements, we have used 10µm, 5µm and 2.5µm grid to demonstrate tip's resolution.

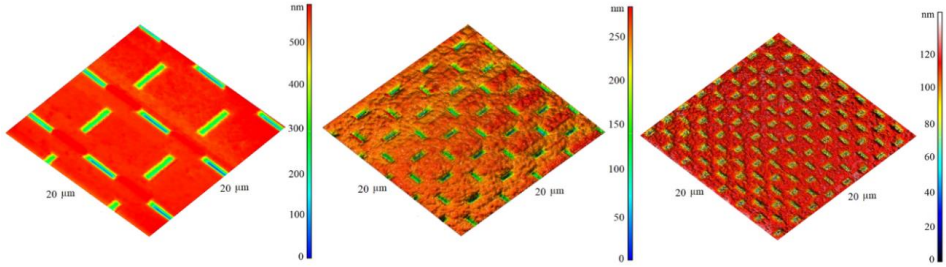

Figure 2.13 SPM image of the special calibration grid showing tip performance and spatial resolution: (left) 10µm grid, (middle) 5µm grid and (right) 2.5 (left) 10 µm grid [A9].

The results of the measurements are illustrated by Figure 2.13 showing three various grid sizes presented above. It can be seen, that in all the grids used a probe was able to follow the surface details precisely and to cover broader area without a change of the spatial sensitivity. By the results presented above, it has been demonstrated that mechanically polished pencil leads are suitable for fast and low-resolution SPM measurements. These probes proved to be reliable for routine characterization of the samples by SPM in air with low resolution of surface features. Cost-effective easy preparations make them useful at education process at laboratory classes of SPM. Generally, a tip made of PG can find an application during education process to scanning probe microscopy techniques or for estimation of topography of conductive samples with high roughness at low resolution of texture details.

3. NOVEL METHODS OF ELECTRON EMITTER CHARACTERIZATION

3.1 NOISE SPECTROSCOPY IMPLEMENTED IN FIELD EMISSION MICROSCOPE

The noise spectroscopy method is one of the non-destructive evaluation methods used especially in semiconductor science and technology [35],[36]. The principle of the method is based on the identification of the main noise components in time- and frequency domain and their assignment to physical phenomena occurring in the system. The most common noise components are $1/f$ noise, generation-recombination (GR) noise, thermal noise and shot noise [36],[37],[38]. Based on our previous findings [39],[40], it can be used not only to characterize the electron emitter, but also to evaluate the function of the entire electron-optical system since the unwanted fluctuations and noises have adverse effect on the electron aberrations and on a detection system in general [41]. The longtime goal of my research is this to fully implement this method for use in a field emission microscope, which is in fact the simplest electron projection system used now mostly for analyzing emission sources [A7]. This chapter also includes a demonstration of the utilization of this method to a more complex system, which is a scanning electron microscope [A10].

The noise spectroscopy method was implemented into field emission microscope to describe the noise and fluctuations of electron beam that is being collected by a coated scintillating crystal inside an ultra-high vacuum chamber [A7]. The setup is illustrated in Figure 3.1.

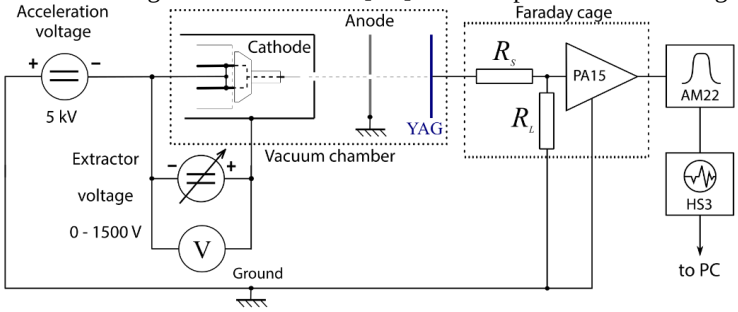

Figure 3.1 Noise measurement implementation into FEM showing the connection of the electron gun and the noise measurement system located within a Faraday cage. The tip to extraction cathode distance is usually between 0.75–1 mm [A7].

A field emission cathode is placed within an extractor electrode embedded within a vacuum chamber (P~10^{-7} Pa) aiming towards an anode which accelerates electrons by high voltage (5 kV). The accelerated electrons are collected on the scintillator electrode made of Cerium doped Yttrium

Aluminum Garnet coated with a conductive layer (20nm Al layer), which allows to display an emission pattern, and to conduct the impinging primary electrons. The measurement part of the set-up is placed outside the vacuum chamber within a Faraday cage shielding the measurement resistors R_S (491 kΩ), R_L (492 kΩ) and the preamplifier PA15 (20 dB) made by 3S Sedlak. The measurement amplifier AM22 is dynamically set based on the output signal level. The AM22 also serves as a filter providing a proper signal for the HS3 oscilloscopic card which samples the signal to the computer [A7].

As it was mentioned in previous chapter, the polymer graphite cathode made by FIB behaves like metal emitter, which is further supported by a I-V and FN plots illustrated in Figure 3.2.

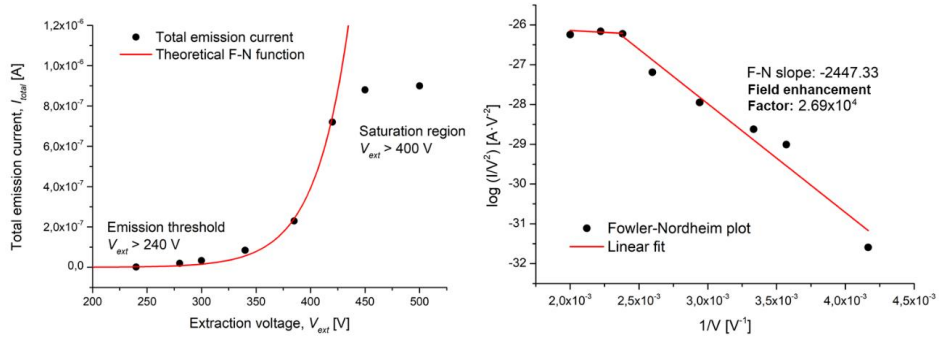

Figure 3.2 The current-voltage characteristics obtained from measurement in FEM (left); The Fowler-Nordheim plot showing F-N slope and field enhancement factor (right) [A7].

The current that is measured on the YAG scintillator in the time domain is transformed into a spectral domain and further analyzed. The noise measurements were obtained using two different extraction voltages representing two determining states of the field emission illustrated in Figure 3.3 (left; V_{ext} = 325 V) and Figure 3.3, (right; V_{ext} = 525 V). According to Figure 3.3 (left), each voltage represents a different operation mode. For V_{ext} = 325, our cathode operates in a regular, unsaturated state and for V_{ext} = 525 V, the cathode operates in a saturation state, which means that for the increased extraction voltage, the emission current does not increase anymore. For both extraction voltages, the thermal noise level is calculated, and its value is given by 4kTR, where T is temperature, R is resistance and k is Boltzmann constant [35]. For our measurement, the 4kTR equals 4.07×10^{-15} V^2s (or V^2/Hz) [A7].

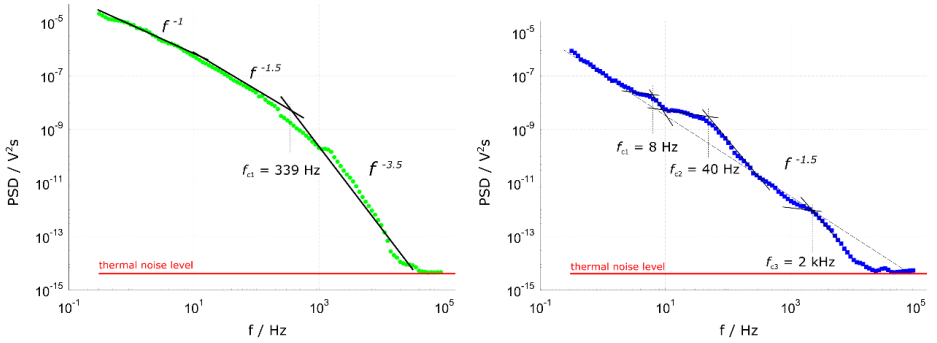

Figure 3.3 Noise power spectral density for the total emission current measured at V_{ext} = 325 V (left) and for V_{ext} = 525 V. Both measurements were done at constant pressure and electron energy [A7].

For V_{ext} = 325 V as illustrated in Figure 3.3 (left), the 1/*f* noise, dominates up to the cut-off frequency f_{c1} = 339 Hz. The 1/*f* noise is a process with a frequency spectrum such that the power spectral density is proportional to the reciprocal of the frequency and has been already studied in numerous papers [37],[38]. As for the lower part of the spectrum where the $1/f^{n}$ noise, where the n parameter is in the range $1.0 \leq n \leq 1.5$ [A7]. The exact value of n is determined by the nature of the recombination, the lifetime probability density function, and by the trap density function. It has been already shown that the trap densities close to the conduction and valence band lead to higher values of n [42]. The cutting frequency is located near the region where the spectrum becomes steeper, which is caused by a superposition of the particular 1/*f* and generation-recombination (GR) processes. Such an effect may be explained by adsorption and desorption of various atoms present with some residual gas in the vacuum chamber, which happens on the tip surface [40]. In the bulk, a volume diffusion (i.e., a diffusion within a single graphite flake) plays a more significant role, especially in the direct vicinity of the emission tip, where the temperature is increased due to electron tunneling. For V_{ext} = 525 V, the spectrum slope shows such an influence, which is probably caused by the increased temperature induced by a higher emission current. The diffusion again takes place along with a GR process caused by particle movement in the bulk towards the tip. The defects contained within the bulk which are probably the polymer particles behave like particle traps with an exponential energy distribution function. There are several cut-off frequencies connected to the particular GR noise components; in particular: 8 Hz, 40 Hz, and 2 kHz [A7].

Based on the presented data, the polymer pencil graphite may be used as a material for preparation of field emission cathodes when operating in a particular voltage regime. It has been shown that the bulk defects, behave like particle traps creating significant generation-recombination noise and hence the volume and surface diffusion which directly affects the number of emitted electrons.

3.2 NOISE SPECTROSCOPY USED TO EVALUATE SCANNING ELECTRON MICROSCOPE

During the implementation of noise spectroscopy in FEM, the idea arose to test this methodology on a complex electron-optical system such as a classical scanning electron microscope, for which we have chosen an older scanning electron microscope (branded Tescan Vega, v.1) [A10]. This microscope was selected because it can be very easily disassembled and contacted through existing set of feedthroughs. As the electron source for this microscope operates in a purely thermal-emission mode, it was not possible to fully assess the effect of electrical noise and fluctuations on the stability of the applied field, however, this was not the focus of the investigation.

Emitted current goes through a column consisting of two condenser lenses, the auxiliary centering lenses and stigmators and a pair of scanning coils. The beam then continues through objective out of the column as illustrated in Figure 3.4. There were two apertures cropping the electron beam and reducing the total emission current approximately thousand times. The electron beam was focused into a Faraday cage through narrow aperture on the top of the cage that was placed under the objective collecting all impinging electrons within [A10]. To reduce a deflection of the beam, the following configuration was set: the beam has been focused to the edge of the Faraday cage and then magnified inside the cage to obtain as smallest field of view. At the highest magnification the area of scanning was minimized to a square covering 5 nm^2, which almost suppressed the beam scanning. By reducing the scanning speed (s) to level s=12, the dwell time (i.e., the period that a beam remains in a same position) for a single pixel is equal to 2.36 ms, therefore, the area of 5 nm^2 (17 squared pixels) is scanned periodically every 0.68 s obtaining continual output current.

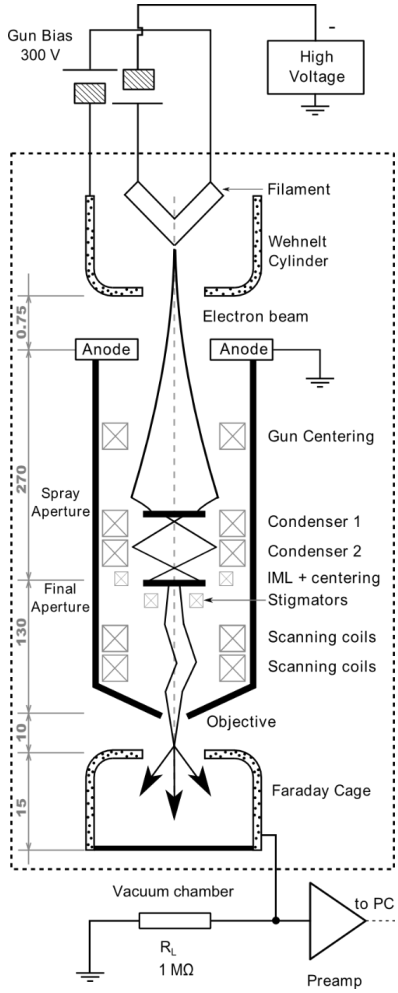

Figure 3.4 Schematic representation of the cathode and optical elements of the scanning electron microscope Tescan Vega (v.1), where left are distances in mm [A10].

Output current of the Faraday cage has been grounded through a 1MΩ resistor on which the voltage fluctuations have been measured. After the voltage on the load resistor stabilizes, the voltage was measured, sampled, and recorded [A10]. The paper describes 3 basic experiments + one additional that are commented on below.

The first measurement was performed on a cathode that was stored for a longtime at the room temperature. In this case the cathode surface was initially covered by thin film of tungsten trioxide that is created during cathode cooling from previous operation. Voltage noise spectral density S_u as a function of frequency is shown in Figure 3.5. The measurement resistor *R* operates at room temperature T=300 K yielding background noise level (BN) equal to 4kTR, as it is plotted in Figure 3.5.

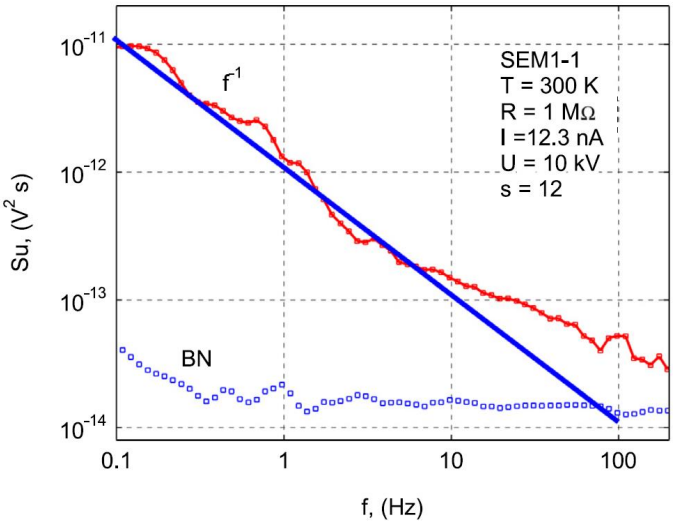

Figure 3.5 The initial voltage noise spectral density for long-time stored cathode that was coated by tungsten oxide; marked as SEM1-1 [A10].

At the frequency range from 0.1 up to 10 Hz is noise spectral density 1/*f* type. The change of the low frequency component is described further in the text. For electron beam with a current of I_{eb} = 9.8 nA, the current noise spectral density $S_i = 3.14 \cdot 10^{-27}$ A^2/Hz because of the shot noise was found. Shot noise may be dominant when the finite number of charged carriers is sufficiently small so that uncertainties due to the Poisson distribution, which describes the occurrence of independent random events, are of significance. In our measurements, the shot noise component is about one order below the mean the obtained current noise spectral and for this reason, the effects of a shot noise were neglected [A10].

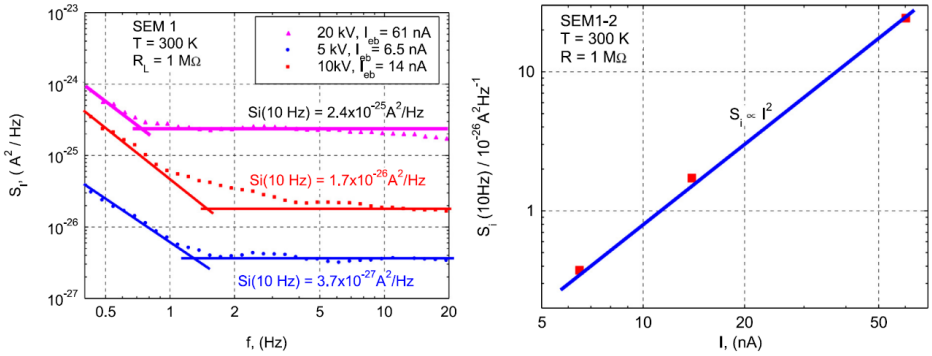

Figure 3.6 Influence of the accelerating voltage: the measured current noise spectral density S_I at anode voltage 5 to 20 kV (left) and the current noise spectral density vs. electron beams current (right) [A10].

The second experiment described in the paper [A10] was performed with various accelerating voltages starting from 5 to 20 kV as it is illustrated in Figure 3.6. Low frequency noise measured was in scale from 0.3 to 1 Hz and was of $1/f^{\,n}$ type where *n* varies from 1 to 2. Low frequency component is changed from 1/*f* spectrum to $1/f^{\,2}$ due to a progressive accumulation of emitted carriers near the cathode surface. These carriers don't have sufficient energy to leave the surface

and move towards the anode. For the period of t =1000 s the voltage noise spectral density is decreasing as is shown in Figure 3.6 [A10]. This phenomenon was explained in a previous paper published along with Sergeev [40], considering those a model of adsorption-desorption noise was formulated based on the Kolmogorov equation [40].

From the measurement illustrated in Figure 3.6 (left), it has been concluded that the current noise spectral density at frequency 10 Hz increased with increasing electron beam current as it is shown in Figure 3.6 (tight). The current noise spectral density increased with a square of current also confirming a supposition that the noise is of a GR type [A10],[40].

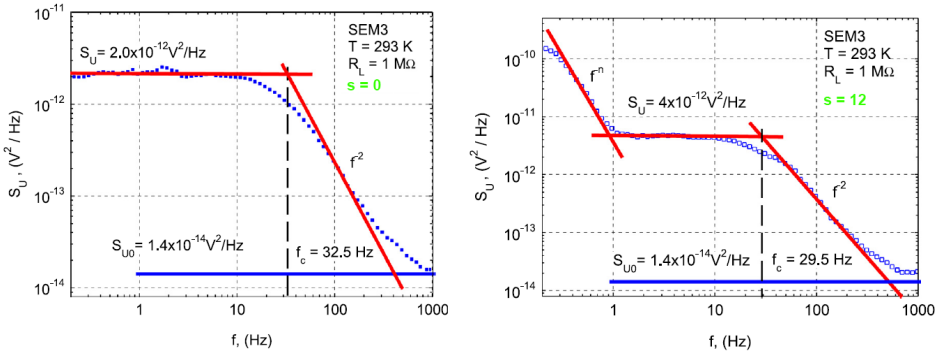

Figure 3.7 Influence of the scanning speed: voltage noise spectral density for measured for s=0 (left) and s=12 (right) [A10].

The third experiment was performed with accelerating voltage 30 kV and special values of voltages on condensers and stigmators. This configuration is described by Figure 3.4. Measured voltage noise spectral density for scanning speed s=0 is GR type as is shown in Figure 3.7 (left). The cut-off frequency in this case is f_c=32.5 Hz and voltage noise spectral density at 1 Hz S_u equal to 2×10^{-12} V^2/Hz, as it is illustrated by Figure 3.7 (left). It is supposed that this GR noise component originates from the electron optics and relates to the electric field distribution among anode, condensers, stigmators and objective as it is illustrated in Figure 3.4. Beam deflectors which are used to scan the electron beam across the specimen consist basically of two scanning coils: one is for horizontals deflection and second one for vertical deflection. Since both operate on frequencies whose overall speed may be set by end-user, the effect of beam deflection has been considered as a possible source of unwanted fluctuations and was further examined. Effect of scanning frequency is shown in Figure 3.7 (right) where f_c=29.5 Hz, which is slightly lower than for the scanning frequency where s=0. Moreover, in the frequency band below 1 Hz, a new source of noise appears. This noise component is related to the electric field distribution between anode and objective and is dependent on the scanning frequency [A10].

The additional experiment dealt with the influence of the filament heating as it is illustrated in in Figure 3.4. The level of the filament heating can be simply chosen from four different presets which are marked as: “weak”, “middle”, “strong” and “extra” offering four levels of a cathode heating. The increase of the heating intensity also increases the total emission current. For each heating level, two spectral measurements were done, which was illustrated in fig. 9 of [A10]. From the spectral density measurements, it was determined that the heat increase is not directly proportional to the mean value and to the shape of the spectral curve is not constant. The explanation is rather straightforward and may be explained in by that the cathode works most smoothly when the “extra heat” option is selected. In this case, the cathode working point is in the region of current saturation, which means that all the available electrons are used for charge transport and any current increase would not increase the emission. This also positively influences the electron emission probability.

3.3 ORTHODOX TESTING IMPLEMENTED IN FIELD EMISSION MICROSCOPE

The orthodox testing methodology based on the updated Fowler-Nordheim theory proved to be another suitable and completely non-destructive method for implementation in focused electron beam devices [43]. The general idea is to implement an automated method whereby a device (such as an electron microscope or electron lithograph) tests the cathode before or after the operation and uses the extracted data to determine cathode parameters related to cathode lifetime and performance. We have recently presented the online implementation in several common papers with Forbes [A11], [A12] and offered it to the public for free use in the form of a website[1]. Version 0.9 is currently available and offers extended functionality implementing features such as: scaling parameters calculator, macroscopic field analysis, macroscopic current density, and current density-field analysis for single tip emitters (SFE) and large area field emission emitters (LAFE). In the future, an implementation tied to a specific type of electron-optical device will be developed to provide continuous information about the emitter state using orthodox testing, which is presented in more detail in the following subsections.

In 1928, the first straight line relation was introduced by R. A. Millikan and C. C. Lauritsen, which is now well known as the Millikan-Lauritsen (ML) plots [47], this type of plots takes the form of $\ln(I_m)$ vs V_m^{-1}. In 1929, a second straight-line relation has been found by T. E. Stern, B. S. Gossling and R. H. Fowler that takes the form of $\ln(I_m/V_m^2)$ vs V_m^{-1}, this is well known as the Fowler-Nordheim (FN) plots [48].

The most modern form of these analysis plots is introduced in 2019 by R. G. Forbes when he introduced the extended Murphy-Good (MG) plots, this is expressed as $\ln(I_m/V_m^{\kappa})$ vs V_m^{-1}, where $\kappa = 2 - \eta/6$ [A11]. Murphy-Good plots theory provides the most nearly exact straight-line form of the analysis plots and is characterized by the absence of the correction factors. For these two reasons, it is more advised to used Murphy-Good method to test and analyze FEE experiments data. In what follows, and for simplicity, $\kappa = 2 - \eta/6$ for MG plots, $\kappa = 2$ for FN plots and $\kappa = 0$ for ML plots.

The field emission orthodoxy test is a *quantitative test* aims to check for the validity and the preciseness of the analysis results. The test uses (commonly trusted) reference data achieved between 1926 to 1972 serving for comparison with the tested data. The procedure includes extracting of the characterization parameters for the test-pass emitters. The characterization parameters that can be extracted from field electron emission current-voltage characteristics are mainly [A12]:

1. *The voltage conversion length* ζ_C , is a mathematical parameter that is used to connect the voltage difference to the corresponding electrostatic field, which give us an information about the change of the curvature of the tip. It can be defined as the distance from the surface of the metal where the local electrostatic field remains uniform. The potential difference across a distance ζ will be equals to $V = E\zeta$.
2. *The field enhancement factor* γ_C, is a mathematical parameter that is used to connect the local electrostatic field to the applied external electrostatic field and can be defined also as the ratio between the local field to the applied field. The physical meaning of γ can be described by its value, since it is used to enhance the E_M so that quantum tunneling through the metal potential barrier for the electrons becomes possible.
3. *The formal emission area* A_f^{SN}, is a mathematical parameter related to the real geometrical/notional area of the emission process. It does not represent the real geometrical

emission area, but it can be connected to $A_n = (A_f/\lambda)$ using an uncertainty factor $0.005 \leq \lambda \leq 14$. In a simple word, it is the area where the electrons leave the surface of the metal to the vacuum. Its value can be less than, larger or equal to A_n.

4. *The formal area efficiency* α_f^{SN}, is the ratio between the formal emission area to the total geometrical macroscopic area of the surface of the emitter of the effective emission area to the total geometrical area $\alpha_f = (A_f/A_M)$. Its physical meaning is clear, the ratio of the contributed area in the emission process.

The orthodoxy testing is based on the presented theory and was originally suggested by Forbes in 2013 based on experimental results provided in generally trusted publications since 1926. The general idea of the concept is to extract the scaled field values from experimental FEE-$I_m(V_m)$ data and compare it to a set of the existing experimental scaled field values. The test results are then used to determine whether the extracted characterization parameters for the used emitter are precise or less precise. Converting the function to a computer function, we have reached the very first practical implementation in the previously mentioned papers prepared along with Forbes [A11], [A12]. The implemented function operates based on extraction of the scaled field values for the upper and lower limits (of an analysis plot) and there apply the test general criteria, to the limits presented in Table 3.1. Followingly, the f_{low}^{A} and f_{low}^{NA} are the lower allowed/not allowed limits f_C^{extr}, and f_{up}^{A} and f_{up}^{NA} are the upper allowed/not allowed limits when compared to f_C^{extr}. The extracted scaled field range limits as a function of the local work function are listed in Table 3.2.

Table 3.1 Field emission Orthodoxy Test general criteria.

General conditions	Test result	Description
$f_{low}^{A} \leq f_C^{extr} \leq f_{up}^{A}$	Pass	The extracted parameters are precise and valid to consider
$f_C^{extr} \leq f_{low}^{NA}$ OR $f_C^{extr} \geq f_{up}^{NA}$	Fail	The extracted parameters are not precise and not valid to consider
$f_{low}^{NA} < f_C^{extr} < f_{low}^{A}$ OR $f_{up}^{A} < f_C^{extr} < f_{up}^{NA}$	Inconclusive	More study and analysis are needed

Table 3.2 The extracted scaled field range limits as a function of the local work function.

Work Function List [eV]	$f^{NA}{}_{low}$	$f^{A}{}_{low}$	$f^{A}{}_{up}$	$f^{NA}{}_{up}$
5.5	0.09	0.14	0.41	0.69
5.0	0.10	0.14	0.43	0.71
4.5	0.10	0.15	0.45	0.75
4.0	0.11	0.16	0.48	0.79
3.5	0.11	0.17	0.51	0.85
3.0	0.12	0.18	0.54	0.91
2.5	0.13	0.20	0.59	0.98

To conclude, the field emission orthodoxy test can be used to check for the status of the used field emitter in various instruments utilizing focused electron beam [A12]. This can be done by monitoring the status of the characterization parameters and the test results.

[1] The public implementation can be found on: **https://fieldemissionanalysis.weebly.com/**

4. CONCLUSIONS AND FUTURE DEVELOPMENT

This habilitation thesis summary is presented in the form of an annotated list of publications that deal with new methods and materials for research on field emission electron emitters. These publications which were produced between 2013 and 2021 dealing with a common topic, which are novel methods leading to the preparation of field emission sources. The research topic is loosely related to and further extends the topic I addressed within the frame of my PhD thesis in 2008-2013.

The publications listed were produced within the framework of partial projects carried out at the Institute of Scientific Instruments of CAS (mainly Technology Agency of Czech Republic, Grant Agency of Czech Republic and SIMDALEE2 project funded by the European Commission) participating within several working groups, which allowed to establish international and interdisciplinary cooperation and therefore to extend the topic beyond the usual disciplinary focus on physics and electrical engineering. Thus, the publications that the author comments on in this thesis are mainly peer-reviewed impacted articles from international journals [A2],[A5],[A6],[A7],[A8],[A9],[A10],[A11], from the peer-reviewed indexed article [A1] and from international conferences [A3],[A4],[A12]. A practical output in a form of a utility model which further extends the paper [A2] is attached to the list [A13].

As mentioned before, the topic is very broad and multidisciplinary, and therefore the primary focus of this thesis has been on methods that are applicable in experimental development and allowing us to obtain samples of functional cathodes, on which the further material research and characterization has been carried out. The method for the fabrication of the cathode and the functional nanotube-based structure is discussed in Chapter 1. Special attention is paid to introduce cathodes with ultra-sharp tips, which are coated with a thin layer of dielectric [A1]. This issue was previously the essence of my PhD thesis and yielded many findings which I lately reinterpreted and correlated with the research results of our Jordanian colleagues, namely Prof. Mousa's laboratory at Mu'tah University in Al-Karak [A1].

In the first chapter, the focus is given to improved methodology for the preparation of classical field-emission tips, which we upgraded to a modern and fully automated way. In the commented paper [A2], a new method of etching is described increasing the repeatability and quality of the obtained tips even from polycrystalline tungsten. This output is of great interest for companies and a commercial prototype is currently being prepared.

In the second part of the first chapter, the lithographic formation of a gate structure for an arbitrary nanotube is described and the growth of a platinum nanotube in this structure is demonstrated as an example [A4]. The design also includes the optimization of the gate structure in terms of electron-optical parameters, which will allow the optimum total emission current and the narrowest possible energy spectrum of the emitted beam [A3].

The second chapter of this thesis deals with new materials that have the potential to be used in the fabrication of field emission cathodes. In the beginning of this chapter, the field emission properties are measured on defects of highly oriented pyrolytic graphite providing promising results despite the relatively high work function of the material [A5]. With these basic results, we have extended the research to polymer graphite, which is a modern composite form of graphite used mainly to produce refills for micro-pencils, but also to produce very efficient electrodes for voltametric measurements [A7],[A8]. Polymer graphite is a very affordable and easy to process material that offers several possible applications in relation to the method by which it is processed. It can work as a classical single-point electron source with metal-like properties. Furthermore, it can function as a multipoint electron source, due to the large number of suitably oriented flakes of graphite from which the emission takes place. Lastly, it can serve as a probe for SPM microscopy techniques, where it scans over the surface of the sample as a probe [A9]. These outputs have been documented as functional samples and subsequently published in impacted publications.

The second chapter also includes the development and characterization of tungsten oxide-based nanotubes, specifically the W_5O_{14} and $W_{18}O_{49}$ phases [A6]. The development of these nanotubes was carried out as part of a large EU project in international scientific cooperation with Slovenia and Switzerland. The author was supervising the measurements for the Czech side and was responsible for the preparation and characterization of the functional samples in microscopic and macroscopic modes. The results of measurements on the obtained nanotube samples demonstrated suitable field emission properties of these materials [A6].

A minor overlap with fundamental research is related to the characterization methodology, which is the subject of the final chapter. This consists of two parts; noise spectroscopy [A7],[A10] and an orthodox testing methodology based on the Murphy-Good formalism [A11], [A12]. The noise spectroscopy method builds on preliminary measurement done within the last chapter of my PhD dissertation where it was first time used for non-destructive characterization of FE tips. Within the papers [A7] and [A10], the method has been further studied and successfully implemented both on a cathode sample (in this thesis we demonstrate its use on a polymer graphite cathode) and within a complex electron-optical system (electron microscope). The research was carried out in the framework of a long-term collaboration with the Czech Noise Research Laboratory led by Professor Šikula at FEEC BUT.

The second method, which is also based on the measurement and analysis of electrical quantities, is being investigated in collaboration with the University of Surrey, specifically with a pioneer in the field, Dr. Richard Forbes. As part of this research, a comprehensive method of testing experimental data has been proposed yielding four essential parameters characterizing the field emitter *in situ*. The very first implementation has been done on a web platform to be available for the professional community [A11], [A12]. In a near future, the implementation should be implemented directly into the control software of an electron microscopy, which should provide a cathode health rating related directly to the four parameters presented and thus inform user when the cathode reaches the end phase of its lifetime.

To conclude, both methods are very suitable as non-destructive, *in situ* methods for diagnosing the function of field emission cathodes, where the cathode does not need to be removed from the vacuum chamber and studied in a complicated manner by other methods.

SELECTED PUBLICATIONS OF THE AUTHOR

[A1] MOUSA, M. S.; KNÁPEK, A.; GRMELA, L. Similarities and Differences between Two Researches in Field Emission of Electrons: A Way to Develop More Powerful Electron Source. *Jordan Journal of Physics*, 2020, 13.2: 171-179, 10.47011/13.2.9.

[A2] KNÁPEK, A. et al. Programmable set-up for electrochemical preparation of STM tips and ultra-sharp field emission cathodes. *Microelectronic Engineering*, 2017, 173: 42-47, 10.1016/j.mee.2017.04.002.

[A3] KNÁPEK, A.; RADLIČKA, T.; KRÁTKÝ, S. Simulation and Optimization of a Carbon Nanotube Electron Source. *Microscopy and Microanalysis*, 2015, 21.S4: 60-65, 10.1017/S1431927615013148.

[A4] BURDA, D.; KNÁPEK, A. Lithographic method of preparing a gating structure for a nanotube-based field mission source. In: *6th IMAPS Flash Conference. Book of Abstracts*. Brno: Brno University of Technology, 2021, ***(in submission/in press)***.

[A5] KNÁPEK, A., et al. Field emission from the surface of highly ordered pyrolytic graphite. *Applied Surface Science*, 2017,395:157-161, 10.1016/j.apsusc.2016.05.002.

[A6] SAQIB, M.; DE PIETRO, L.; KNÁPEK, A. et al. Field emission properties of single crystalline W_5O_{14} and $W_{18}O_{49}$ nanowires. *Journal of Electron Spectroscopy and Related Phenomena*, 2020, 241: 146837, 10.1016/j.elspec.2019.03.005.

[A7] KNÁPEK, A., et al. Preparation and noise analysis of polymer graphite cathode. *Metrology and Measurement Systems*, 2018, 25.3. 10.24425/123895

[A8] KNÁPEK, A., et al. Field emission properties of polymer graphite tips prepared by membrane electrochemical etching. *Nanomaterials*, 2020, 10.7: 1294, 10.3390/nano10071294

[A9] KNÁPEK, A., et al. Polymer graphite pencil lead as a cheap alternative for classic conductive SPM probes. *Nanomaterials*, 2019, 9.12: 1756. 10.3390/nano9121756

[A10] KNÁPEK, A.; ŠIKULA, J.; BARTLOVÁ, M. Fluctuations of focused el. beam in a conventional SEM. *Ultramicroscopy*, 2019, 204: 49-54, 10.1016/j.ultramic.2019.05.008

[A11] ALLAHAM, M. M.; FORBES, R. G.; KNÁPEK, A.; MOUSA, M. S. Implementation of the orthodoxy test as a validity check on experimental field emission data. *Journal of Electrical Engineering* 71, no.1 (2020): 37-42, 10.2478/jee-2020-0005

[A12] ALLAHAM, M. M.; KNÁPEK, A.; MOUSA, M. S.; FORBES, R. G. User-friendly method for testing field electron emission data: Technical report. In: Proceedings of 34th International Vacuum Nanoelectronics Conference (IVNC2021), 2021: 138-139.

[A13] ÚSTAV PŘÍSTROJOVÉ TECHNIKY AV ČR, V. V. I. Zařízení pro opakovatelnou výrobu ostrých hrotů [Device for repeatable production of sharp points]. Originators: Alexandr KNÁPEK, Pavel KLEIN, Armin DELONG.
Czech Republic. Užitný vzor [Utility model] CZ 33278 U1.7.10.2019.

REFERENCES[2]

[1] FOWLER, R. H.; NORDHEIM, L. W. Electron emission in intense electric fields. *Proceedings of the Royal Society of London. Series A*, Containing Papers of a Mathematical and Physical Character, 1928, 119.781: 173-181.

[2] NORDHEIM, L. W. The effect of the image force on the emission and reflexion of electrons by metals. *Proceedings of the Royal Society of London. Series A, Containing Papers of a Mathematical and Physical Character*, 1928, 121.788: 626-639.

[3] ECKERTOVÁ, L.; FRANK, L. Metody analýzy povrchů: elektronová mikroskopie a difrakce [Methods of surface analysis: electron microscopy and diffraction]. 1. ed. Prague: Academia, 1996, 379 p. ISBN 80-200-0329-0.

[4] MELMED, A. J. The art and science and other aspects of making sharp tips. *Journal of Vacuum Science & Technology B*: Microelectronics and Nanometer Structures Processing, Measurement, and Phenomena, 1991, 9.2: 601-608.

[5] IBE, J. P., et al. On the electrochemical etching of tips for scanning tunneling microscopy. *Journal of Vacuum Science & Technology A*: Vacuum, Surfaces, and Films, 1990, 8.4: 3570-3575.

[6] EKVALL, I., et al. Preparation and characterization of electrochemically etched W tips for STM. *Measurement Science and Technology*, 1999, 10.1: 11.

[7] YU, Z. Q., et al. Reproducible tip fabrication and cleaning for UHV STM. *Ultramicroscopy*, 2008, 108.9: 873-877.

[8] FRANSEN, M. F. *Towards high-brightness, monochromatic electron sources*. TU Delft, Delft University of Technology, 1999.

[9] MÜLLER, E. W. Work function of tungsten single crystal planes measured by the field emission microscope. *Journal of Applied Physics*, 1955, 26.6: 732-737.

[10] CUI, Z. Nanofabrication: Principles, Capabilities and Limits: Second. DOI: 10: 978-3.

[11] RAI-CHOUDHURY, P. *Handbook of Microlithography, Micromachining, and Microfabrication: Micromachining and Microfabrication*. SPIE Press, 1997.

[12] BALASUBRAMANIAN, K.; BURGHARD, M. Electrochemically functionalized carbon nanotubes for device applications. *Journal of Materials Chemistry*, 2008, 18.26: 3071-3083.

[13] RADLIČKA, T.; LENCOVÁ, B. Coulomb interactions in Ga LMIS. *Ultramicroscopy*, 2008, 108.5: 445-454.

[14] DE TERESA, J. M., et al. Origin of the difference in the resistivity of as-grown focused-ion- and focused-electron-beam-induced Pt nanodeposits. *Journal of Nanomaterials*, 2009.

[15] MÜLLEROVÁ, I.; FRANK, L. Scanning low-energy electron microscopy. *Advances in imaging and electron physics*, 2003, 128: 310-445.

[16] GESHEVA, K., et al. Technologies for deposition of transition metal oxide thin films: application as functional layers in "Smart windows" and photocatalytic systems. In: *Journal of Physics: Conference Series*. IOP Publishing, 2016. p. 012011.

[17] GAVANIER, B.; MICHALAK, F. M.; OWEN, J. R. Electrochemistry of WO_3 based smart windows: Beliefs and facts. *Ionics*, 1997, 3.3: 265-269.

[2] The following references are only cited in the full text of this thesis: 9, 16-21, 23-28, 32, 44-46, 49-50

[18] LADOUCEUR, M., et al. Plasma-sprayed semiconductor electrodes: photoelectrochemical characterization and ammonia photoproduction by substoichiometric tungsten oxides. *Journal of Physical Chemistry*, 1990, 94.11: 4579-4587.
[19] HUANG, Z., et al. Tungsten oxides for photocatalysis, electrochemistry, and phototherapy. *Advanced Materials*, 2015, 27.36: 5309-5327.
[20] LOCHERER, K. R.; SWAINSON, I. P.; SALJE, E. K. H. Phase transitions in tungsten trioxide at high temperatures-a new look. *Journal of Physics: Condensed Matter*, 1999, 11.35: 6737.
[21] MCCOLM, I. J.; STEADMAN, R.; WILSON, S. J. Iron-promoted phases in the tungsten-oxygen system. *Journal of Solid State Chemistry*, 1978, 23.1-2: 33-42.
[22] REMŠKAR, M., et al. W5O14 Nanowires. Advanced Functional Materials, 2007, 17.12: 1974-1978.
[23] WANG, F.; DI VALENTIN, C.; PACCHIONI, G.. Electronic and structural properties of WO3: a systematic hybrid DFT study. *The Journal of Physical Chemistry C*, 2011, 115.16: 8345-8353.Hirose
[24] HIROSE, T.; KAWANO, I.; NIINO, M. Electrical conductivity of tungsten trioxide (WO_3). *Journal of the Physical Society of Japan*, 1972, 33.1: 272-272.
[25] HU, Z., et al. K-enriched WO_3 nanobundles: high electrical conductivity and photocurrent with controlled polarity. *ACS applied materials & interfaces*, 2013, 5.11: 4731-4738.
[26] VISWANATHAN, K.; BRANDT, K.; SALJE, E. Crystal structure and charge carrier concentration of $W_{18}O_{49}$. *Journal of Solid State Chemistry*, 1981, 36.1: 45-51.
[27] BOOTH, J., et al. Notes on phases occurring in the binary tungsten-oxygen system. *Journal of Solid State Chemistry*, 1982, 41.3: 293-307.
[28] DEAN, K. A.; CHALAMALA, B. R. Current saturation mechanisms in carbon nanotube field emitters. *Applied Physics Letters*, 2000, 76.3: 375-377.
[29] PURUSHOTHAMA, H. T.; NAYAKA, Y. Arthoba. Pencil graphite electrode based electrochemical system for the investigation of antihypertensive drug hydrochlorothiazide: An electrochemical study. *Chemical Physics Letters*, 2019, 734: 136718.
[30] RIMAN, D., et al. Low-cost pencil graphite-based electrochemical detector for HPLC with near-coulometric efficiency. *Sensors and Actuators B: Chemical*, 2019, 296: 126618.
[31] NAVRATIL, R., et al. Polymer lead pencil graphite as electrode material: Voltammetric, XPS and Raman study. *Journal of Electroanalytical Chemistry*, 2016, 783: 152-160.
[32] KIM, Y., et al. Measurement of hardness and friction properties of pencil leads for quantification of pencil hardness test. *Advances in Applied Ceramics*, 2016, 115.8: 443-448.
[33] FERRARI, A. C. Raman spectroscopy of graphene and graphite: Disorder, electron–phonon coupling, doping and nonadiabatic effects. *Solid state communications*, 2007, 143.1-2: 47-57.
[34] KARIUKI, J. K. An electrochemical and spectroscopic characterization of pencil graphite electrodes. *Journal of the Electrochemical Society*, 2012, 159.9: H747.
[35] SIKULA, J. and M. LEVINSHTEIN. *Advanced experimental methods for noise research in nanoscale electronic devices*. Boston: Kluwer Academic Publishers, 2004. ISBN 14-020-2170-4.
[36] VASILESCU, G. *Electronic noise and interfering signals: principles and applications*. New York: Springer-Verlag, c2005, xviii, 709 p. ISBN 35-404-0741-3.

[37] DUTTA, P. and P. HORN. *Low-frequency fluctuations in solids: 1/f noise. Reviews of Modern Physics*. 1981, vol. 53, iss. 3, p. 497-516. ISSN 0034-6861. DOI: 10.1103/RevModPhys.53.497.
[38] HANDEL, P. Quantum approach to 1/*f* noise. *Physical Review A*. 1980, vol. 22, iss. 2, p. 745-757. ISSN 0556-2791. DOI: 10.1103/PhysRevA.22.745.
[39] KNÁPEK, Alexandr, et al. Cold field-emission cathode noise analysis. *Metrology and Measurement Systems*, 2012, 19.2: 417-422.
[40] SERGEEV, E., et al. Noise diagnostic method of experimental cold field-emission cathodes. In: *2013 22nd International Conference on Noise and Fluctuations (ICNF)*. IEEE, 2013. p. 1-4.
[41] HAWKES, P.W. and E. KASPER. *Electron optics. 2*. Engl. ed., rev. Oxford: Pergamon Pr, 1972. ISBN 978-008-0162-287.
[42] MOHAMMADI, S.; PAVLIDIS, D. A nonfundamental theory of low-frequency noise in semiconductor devices. *IEEE Trans. on Electron Devices*, 2000, 47.11: 2009-2017.
[43] BURGESS, R. E.; KROEMER, H.; HOUSTON, J. M. Corrected values of Fowler-Nordheim field emission functions v (y) and s (y). *Physical Review*, 1953, 90.4: 515.
[44] MURPHY, E. L.; GOOD JR, R. H. Thermionic emission, field emission, and the transition region. *Physical review*, 1956, 102.6: 1464
[45] FORBES, R. G. The Murphy–Good plot: A better method of analysing field emission data. *Royal Society open science*, 2019, 6.12: 190912.
[46] FORBES, R. G. Development of a simple quantitative test for lack of field emission orthodoxy. *Proceedings of the Royal Society A: Mathematical, Physical and Engineering Sciences*, 2013, 469.2158: 20130271.
[47] MILLIKAN, R. A.; LAURITSEN, C. C. Relations of field-currents to thermionic-currents. *Proceedings of the National Academy of Sciences of the United States of America*, 1928, 14.1: 45.
[48] STERN, T. E.; GOSSLING, B. S.; FOWLER, Ralph Howard. Further studies in the emission of electrons from cold metals. *Proceedings of the Royal Society of London. Series A, Containing Papers of a Mathematical and Physical Character*, 1929, 124.795: 699-723.
[49] ALLAHAM, M. M.; FORBES, R. G.; MOUSA, M. S. (2020), Applying the Field Emission Orthodoxy Test to Murphy-Good Plots. *Jordan journal of Physics*, Volume 13, Number 2. pp. 101-111.
[50] ALLAHAM, M. M.; MOUSA, M. S.; FORBES, R. G. Comparing the performance of Fowler-Nordheim plots and Murphy-Good plots. In: *2020 33rd International Vacuum Nanoelectronics Conference (IVNC)*. IEEE, 2020. p. 1-2.

ABSTRACT

This habilitation thesis focuses on advanced methods for the preparation and characterization of field emission cathodes operating at room temperature and acting as a source of free electrons to the vacuum. Since the preparation and characterization of the field emission sources is a highly multidisciplinary field, combining knowledge from solid-state physics, particle physics, physical statistics, inorganic chemistry and of course the electrical engineering, several technological and analytical methods need to be covered, which is the goal of this work. Although the tunnel effect has been known for more than a century, there is still no widespread electron source that is built purely on the influence of the electric field and is sufficiently stable. The publications annotated in this paper cover the solution of partial problems associated with the development and characterization of new types of field emission sources, at several levels.

First and foremost is a repeatable technical method for forming a sharp tip from polycrystalline tungsten. Then, a methodology for the optimization and preparation of a new lithographic structure, intended to work with a nanotube-based cathode, is proposed. As an alternative to conventional carbon nanotubes, a newly developed tungsten oxide-based nanotube was also used in this work. In the next part of the thesis, the study of new materials moves from tungsten to carbon allotropes; to graphite, or so-called polymer graphite, which appears to be a very interesting alternative to the currently very popular graphene. The final part of the thesis is devoted to characterization field emission microscope compatible methods focusing on the characterization of field emission sources based on total emission current measurements. This involves noise spectroscopy, as well as the method of analysis of the total emission current based on orthodox testing, which can be implemented to field emission microscope or any existing device utilizing focused electron beam and thus to extend its function by a sort of self-diagnostic function.

ABSTRAKT

Tato habilitační práce se věnuje pokročilým metodám přípravy a charakterizace autoemisních katod, pracujících za pokojové teploty a sloužících jako zdroj volných elektronů do vakua. Jelikož příprava a charakterizace autoemisních zdrojů je vysoce multioborová záležitost, která slučuje poznatky z oborů jako jsou fyzika pevné fáze, fyzika částic, fyzikální statistika, anorganická chemie a samozřejmě elektrotechnika, je zapotřebí pokrýt řadu technologických a analytických metod, což si klade za cíl tato práce. Přestože tunelový jev je známý déle než sto let, dosud neexistuje rozšířený zdroj elektronů, který by byl postavený čistě na vlivu elektrického pole a byl dostatečně stabilní. Publikace komentované v této práci pokrývají řešení dílčích problémů spjatých s vývojem a charakteristikou nových druhů autoemisních zdrojů, a to na několika úrovních.

V prvé řadě se jedná o opakovatelnou technickou metodu formování ostrého hrotu z polykrystalického wolframu, dále se jedná o návrh metodiky optimalizace a přípravy nové litografické struktury, určené pro práci s katodou na bázi nanotrubky. Jako alternativa ke klasickým uhlíkovým nanotrubkám je v této práci využita i nově vyvinutá nanotrubka na bázi oxidů wolframu. V další části práce se studium nových materiálů přesouvá od wolframu k alotropům uhlíku. Konkrétně se jedná o grafit, resp. polymerní grafit, který se jeví jako velmi zajímavá alternativa k dnes velmi populárnímu grafénu. Závěrečná část práce se věnuje metodikám charakterizace kompatibilním s autoemisním (projekčním) mikroskopem zaměřujíce se na charakteristiku autoemisních zdrojů na základně měření proudu totální emise. Jedná se o šumovou spektroskopii, a dále na metodě analýzy proudu totální emise na bázi ortodoxního testování, kterou lze implementovat do autoemisního (projekčního) mikroskopu nebo jakéhokoli stávajícího zařízení, které využívá fokusovaný elektronový svazek a rozšířit tak jeho funkcionalitu o vhodnou autodiagnostickou funkci.